

# AI-based Aortic Vessel Tree Segmentation for Cardiovascular Diseases Treatment: Status Quo

Yuan Jin<sup>a,b,c</sup>, Antonio Pepe<sup>a,b</sup>, Jianning Li<sup>a,b,d</sup>, Christina Gsaxner<sup>a,b</sup>, Fen-hua Zhao<sup>e</sup>,  
Kelsey L. Pomykala<sup>d</sup>, Jens Kleesiek<sup>d,f,g</sup>, Alejandro F. Frangi<sup>h,i</sup>, Jan Egger<sup>a,b,d,f,\*</sup>

<sup>a</sup>*Institute of Computer Graphics and Vision, Graz University of Technology, Inffeldgasse 16, 8010 Graz, Austria*

<sup>b</sup>*Computer Algorithms for Medicine Laboratory, Graz, Austria*

<sup>c</sup>*Research Center for Connected Healthcare Big Data, ZhejiangLab, Hangzhou, Zhejiang, 311121 China*

<sup>d</sup>*Institute for AI in Medicine (IKIM), University Medicine Essen (AöR), Girardetstraße 2, 45131 Essen, Germany*

<sup>e</sup>*Department of Radiology, Affiliated Dongyang Hospital of Wenzhou Medical University, Dongyang, Zhejiang, 322100 China*

<sup>f</sup>*Cancer Research Center Cologne Essen (CCCE), University Medicine Essen (AöR), Hufelandstraße 55, 45147 Essen, Germany*

<sup>g</sup>*German Cancer Consortium (DKTK), Partner Site Essen, Hufelandstraße 55, 45147 Essen, Germany*

<sup>h</sup>*Centre for Computational Imaging and Simulation Technologies in Biomedicine (CISTIB), School of Computing, University of Leeds, Leeds, UK*

<sup>i</sup>*Biomedical Imaging Department, Leeds Institute for Cardiovascular and Metabolic Medicine (LICAMM), School of Medicine, University of Leeds, Leeds, UK*

---

## Abstract

The aortic vessel tree is composed of the aorta and its branching arteries, and plays a key role in supplying the whole body with blood. Aortic diseases, like aneurysms or dissections, can lead to an aortic rupture, whose treatment with open surgery is highly risky. Therefore, patients commonly undergo drug treatment under constant monitoring, which requires regular inspections of the vessels through imaging. The standard imaging modality for diagnosis and monitoring is computed tomography (CT), which can provide a detailed picture of the aorta and its branching vessels if completed with a contrast agent, called CT angiography (CTA). Optimally, the whole aortic vessel tree geometry from consecutive CTAs is overlaid and compared. This allows not only detection of changes in the aorta, but also of its branches, caused by the primary pathology or newly developed. When performed manually, this reconstruction requires slice by slice contouring, which could easily take a whole day for a single aortic vessel tree, and is therefore not feasible in clinical practice. Automatic or semi-automatic vessel tree segmentation algorithms, however, can complete this task in a fraction of the manual execution time and run in parallel to the clinical routine of the clinicians. In this paper, we systematically review computing techniques for the automatic and semi-automatic segmentation of the aortic vessel tree. The review concludes with an in-depth discussion on how close these state-of-the-art approaches are to an application in clinical practice and how active this research field is, taking into account the number of publications, datasets and challenges.

**Keywords:** Aorta, Vessel Tree, Machine Learning, Deep Learning, Segmentation, Analysis, Cardiovascular Diseases, Aneurysm, Dissection, Computed Tomography.

## 1. Introduction

The aorta is the largest artery in the human body. It is supplied by the left ventricle and consists of four main sections – ascending aorta, aortic arch, descending thoracic aorta, and abdominal aorta. A schematic image is shown in Figure 1 and Table 1. The aorta delivers oxygen-rich blood from the heart to the whole body. Hence, diseases of the aorta, such as aneurysms, stenosis and dissections, can pose a significant threat to a patient’s life. Non-invasive examinations of the aorta are therefore crucial for early detection and monitoring of these diseases (Nienaber (2013); Tortora and Nielsen (2016)).

These non-invasive examinations include computed tomography and magnetic resonance imaging, with or without contrast agents (Nienaber (2013); Tortora and Nielsen (2016); Nienaber et al. (2016); Pepe et al. (2020)). Segmentation of the whole aorta and all its branches, also named aortic vessel tree segmentation, is critically important during clinical examination of non-invasive vascular imaging (Mistelbauer et al. (2016); Gamechi et al. (2019); Hahn et al. (2020)). Compared with common analysis of two-dimensional slices, the 3D reconstruction of the aortic vessel tree provides a more intuitive and comprehensive visualization. It can help radiologists visualize the whole aorta before examining the single cross-sectional images and help generate broad overviews that aid in CT comparison aimed at identifying disease progression (Mistelbauer et al. (2016)). In addition, the aortic vessel tree helps patients better understand their condition, which can support the communication between doctors and patients (Ritter et al. (2006); Lawonn et al. (2018)).

Table 1: Aortic vessel tree and its main branches (the vessel labels are used in Figure 1).

Label	Name
1	Ascending aorta
2	Aortic arch
3	Descending thoracic aorta
4	Abdominal aorta
5	Brachiocephalic trunk
6	Left common carotid
7	Left subclavian artery
8	Intercostal arteries
9	Celiac trunk
10	Superior mesenteric artery
11	Left renal artery
12	Right renal artery
13	Inferior mesenteric artery
14	Right iliac artery
15	Left iliac artery

---

\*Corresponding author: Jan Egger (egger@tugraz.at)

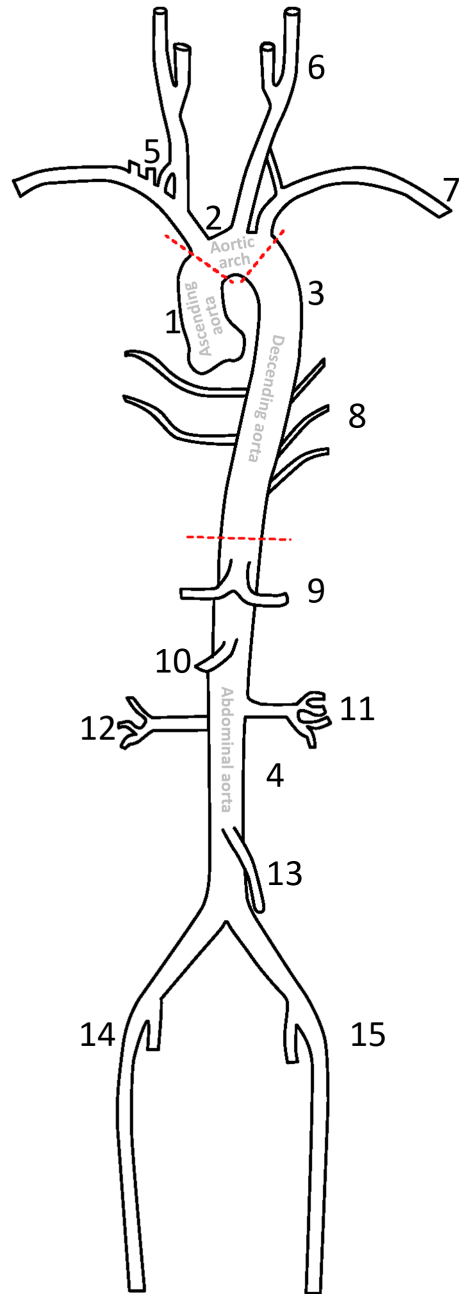


Figure 1: Aortic vessel tree and its main branches and labels (based on the aortic vessel tree and labels of Du et al. (2015)). Please see Table 1 for the corresponding labels. The figure also shows the main aortic segments – separated by red dashed lines – according to Erbel and Aboyans (2014), originating from (the left ventricle) of the heart, extending down to the abdomen, where it splits into the common iliac arteries (labels 14 and 15): Ascending aorta, aortic arch, descending aorta and abdominal aorta. Image courtesy of Xiaoyan Zhou.



Figure 2: Sagittal views for computed tomography (CT, left), computed tomography angiography (CTA, middle) and magnetic resonance angiography (MRA, right) images. The arrows refer to the aorta, which is most visible (brighter) with a contrast agent (CTA and MRA). Datasets taken from SegTHOR database (Trullo et al. (2017); Lambert et al. (2020)), CAD-PE Challenge [<http://www.cad-pe.org/>] and Medical Segmentation Decathlon (Simpson et al. (2019)), respectively.

Medical imaging techniques, such as computed tomography (CT), computed tomography angiography (CTA), magnetic resonance imaging (MRI) and magnetic resonance angiography (MRA), can produce 3D images of the body and are usually employed to examine the patient for aortic diseases, as shown in Figure 2. Depending on the technology, medical images show a range of different internal anatomical structures. The observation of the aorta in the medical images is generally performed by experts, such as vascular radiologists. These need quantitative information about the aortic caliber and, hence, ideally a segmentation of the aorta and its branch vessels from the original medical images (Erbel and Aboyans (2014)).

Manual segmentation of the aorta is a time-consuming task and may lack reproducibility (Gamechi et al. (2019); Hahn et al. (2020)). From the last century, researchers have been working on segmenting vessels from raw medical images. In 1998, Frangi et al. (1998) developed a vessel enhancement filter based on all eigenvalues of the Hessian matrix. In this study the developed filter has been applied to segment the aorta from 3D MRA images (Figure 3, left). In 2000, Krissian et al. (2000) proposed a model-based approach to reconstruct 3D tubular structures and extract their centerlines. The approach was tested based on real 2D X-ray subtracted angiographies and MRA images of brain vessels. In 2005, Pock et al. (2005) further developed a robust tube detection filter for 3D centerline extraction. The authors have compared their method with the previous two from Frangi et al. (1998) and Krissian et al. (2000). Finally, in 2010, Bauer et al. (2010) presented a novel approach for tubular tree structures segmentation, utilizing shape priors and graph cuts (Boykov et al. (2001)). A visual comparison of the results from Frangi et al. (1998) and Bauer et al. (2010) is demonstrated in Figure 3.

These works can mostly be seen as important pre-processing steps that extract or enhance tubular-like structures in raw (medical) images, which are, in fact, mostly vessels. A particular exception is given by diseases that asymmetrically deform original



Figure 3: Vesselness filter results for the aortic vessel tree. Left: Result for a contrast enhanced (gadopen-tetic acid) MRA (magnetic resonance angiography) from Frangi et al. (1998). Right: Result for a contrast enhanced CT dataset from Bauer et al. (2010). *Per se*, these vesselness filters can be seen as a pre-processing step to a subsequent semantic segmentation that adds labels to the single vessels and vessel sections.

shape of a blood vessel, like aortic dissections. However, these are rare, and most vessels keep their tubular structure, even when developing a pathology that deforms their structure like some aneurysms and stenoses. Nevertheless, *per se* these so-called *vesselness* filters do not provide any semantic information, which means they do not label and identify single vessels or vessel sections.

Further semi-automatic or automatic aorta segmentation methods, however, require experts or ground truth images to evaluate their quality. However, these algorithms can greatly assist clinicians, and thus, they are currently one of the most investigated topics in medical imaging. The goal of this contribution is to review different aorta segmentation algorithms, summarize their strengths and limitations regarding segmentation accuracy, computational complexity and fields of application.

We give a comprehensive review of state-of-the-art approaches for aorta segmentation. The goal is to help implement better aortic vessel tree segmentation approaches, as well as to:

1. Discuss detailed evaluation criteria for aortic vessel tree segmentation;
2. Evaluate and conclude the best state-of-the-art approach for this task;
3. Conclude the main challenges and future directions for this task.

**Manuscript Outline.** In the following, section 3 provides an overview of different studies on aorta segmentation, with a breakdown of the segmented aortic parts and clinical-grade morbidities. Table 2 also provides a brief summary of this section. section 4, instead, provides a review of these papers and classifies them into four main categories based on the algorithms involved: deformable model approaches, tracking approaches, deep learning approaches and additional approaches. Types and amount of input data, evaluation metrics, and other functional parameters are also taken into account, which are presented in detail in Table 3, Table 4, Table 5, and Table 6. Several fields of applications for the segmented aortic volumes are then discussed in section 5, followed by a conclusion with new directions for future work in section 6.

**Search Strategy, Inclusion and Exclusion Criteria.** According to the Systematic Reviews and Meta-analyses Protocols guidelines Shamseer et al. (2015), we first performed a systematic search in IEEE Xplore, PubMed, ScienceDirect and Google Scholar for the keywords ‘aorta’ and ‘segmentation’. During the search, we retrieved 833 non-distinct records, and considered six additional papers, which were already known to us. Based on the titles and abstracts, papers with clinical contributions only, such as measurements of the aortic caliber and other medical findings, were excluded (e.g., Morris et al. (2019)). After this step, we assessed the resulting 131 distinct papers and excluded 87 of them. This exclusion was mostly due to the overlap of content (segmentation workflow and approach) with other papers or the lack of quantitative segmentation results. The remaining 44 papers will be presented within this contribution<sup>1</sup>. To the best of our knowledge, this is the first systematic review that gives a thorough analysis of all published aortic vessel tree segmentation papers.

---

<sup>1</sup>More information on the search strategy and results can be found in the supplementary material.

## **2. Aortic Vessel Tree Segmentation: Overview and Challenges**

There are several factors that influence the design of an aortic vessel tree segmentation model, including the type of medical imaging techniques (e.g. CT or MRI), the field-of-view of the radiological examination (e.g., thoracic or abdominal scan), and the underlying segmentation approach. Table 2 organizes studies of aorta segmentation approaches with respect to the parts of the aortic vessel tree segmented.

Table 2: Overview of the reviewed publications according to which parts of the aortic vessel tree they segmented (the vessel labels correspond to the ones in Figure 1) and main diseases involved: Calcifications, aneurysms, or aortic dissections. The publications are ordered and split into four sections according to the other tables in the manuscript: deformable model algorithms (Table 3), tracking algorithms (Table 4), deep learning algorithms (Table 5) and additional algorithms (Table 6).

	Study	No disease	Calcifications	Aneurysms	Aortic dissections
∞	Rueckert et al. (1997)	1			
	Loncaric et al. (2000)			4	
	Subasic et al. (2000)			4	
	Olabarriaga et al. (2005)			4	
	Das et al. (2006)			4	
	Zhuge et al. (2006)			4	
	Kim et al. (2007)			4	
	Herment et al. (2010)	1,3			
	Auer and Gasser (2010)			4,14,15	
	Krissian et al. (2014)				1,2,3,4,5,6,7,12,13,14,15
	Kurugol et al. (2015)		1,2,3,4		
	Bustamante et al. (2015)	1,2,3,4,5,6,7			
	Volonghi et al. (2016)	1,2,3,4,5,6,7			
	Gao et al. (2016)	1,2,3,4,14,15			
	Duan et al. (2016)				1,2,3,4
	Morais et al. (2017)	1,2,3,4			
	Wang et al. (2017)			4,14,15	
	Bidhult et al. (2019)	1			
	Lareyre et al. (2019)			4,11,12,13,14,15	
	Kosasih (2020)			4	
	Subramanyan et al. (2003)			4,13,14,15	
	Boskamp et al. (2004)	4,15			

continued



Table 2 (continued)

Study	No disease	Calcifications	Aneurysms	Aortic dissections
Zheng et al. (2010)	1,2,3,			
Biesdorf et al. (2011)	1,2,3,4			
Martínez-Mera et al. (2013)	1,2,3,4,5,6,7,10,11,12,13			
Xie et al. (2014)	1,2,3,4			
Selver and Kavur (2016)			4,9,11,12,14,15	
Tahoces et al. (2019)	1,2,3,4			
Trullo et al. (2017)	1,2,3,4			
López-Linares et al. (2018)			4	
Li et al. (2019)				1,2,3,4
Cao et al. (2019)				1,2,3,4
Fantazzini et al. (2020)	1,2,3,4,5,6,7,12,13,14,15			
Howard et al. (2020)	1,2,3,4			
Hepp et al. (2020)	1,2,3,4			
Berhane et al. (2020)	1,2,3,4,5,6,7,10			
Hahn et al. (2020)				1,2,3,4
Chen et al. (2021)				1,2,3,4,5,6,7,10,11,12,13,14,15
Yu et al. (2021)				1,2,3,4
Jin et al. (2021)	1,2,3,4,5,6,7			
Zhong et al. (2021)	1,2,3,4,5,6,7			
Cheung et al. (2021)	1			
de Bruijne et al. (2002)			4	
Bodur et al. (2007)			1,2,3,4	
Duquette et al. (2012)			4	
Freiman et al. (2012)	1,2,3,5,6,7			

continued

Table 2 (continued)				
Study	No disease	Calcifications	Aneurysms	Aortic dissections
Bustamante et al. (2015)	1,2,3,5,6,7			
Gamechi et al. (2019)	1,2,3,4			

Based on our review, there are only a few studies focused on semi- or fully automatic segmentation of whole aortic vessel trees Shahzad et al. (2015); Chen et al. (2021). To the best of our knowledge, there could be several reasons behind this.

- Lack of original datasets (Pepe et al. (2020)). Tasks of whole aortic vessel tree segmentation require large amounts of raw data. Scanning should include both thorax and abdomen, which also means a longer scanning duration and higher radiation dose for CTs. Due to the potentially harmful effects of ionizing radiation, this should be limited to retrospective imaging.
- Lack of segmentation masks as ground truth. The generation of ground truth masks for aortic trees is expensive, as documented by Hahn et al. (2020).
- Image noise as a major problem during automatic segmentation. Newly acquired images might present a different amount of noise compared to the original training sets. Thoracic pain, common in many vasculopathies, often limits a patient's ability to remain still during image acquisition and/or hold their breath, and, together with the movements of the physiological heartbeat can lead to motion artifacts (Barrett and Keat (2004); Gallagher and Raff (2008)).

### 3. Aortic Pathologies: Clinical Workflow, Implication and Relevance

As the largest artery in the human body, diseases of the aorta can lead to serious complications (Maton et al. (1995)). The aorta and its branches can be involved in several different pathologies and abnormalities: acute aortic syndromes, aortic aneurysms, atherosclerosis, aortic rupture, pseudoaneurysms, inflammatory diseases, genetic diseases as well as congenital abnormalities (Erbel and Aboyans (2014)). In this section, we introduce some common aortic diseases.

The name of **acute aortic syndrome (AAS)** refers to aortic pathologies that involve the aortic wall (Tsai et al. (2005)). These include aortic dissection (AD), intramural hematoma (IMH), and penetrating atherosclerotic ulcer (PAU), the most common of which is AD (85% to 95% of all AAS) (Harris et al. (2012)).

In a classical sense, **aortic dissection** is the consequence of a tear in the aortic intima. Blood passes through the tear separating the intima from the media and adventitia, creating a false lumen (Khan and Nair (2002)). Evidence showed that the tear often follows a degenerative or necrotic process of the aortic media (Levy et al. (2022); Osada et al. (2018); Wu et al. (2013)). Depending on the location of this tear, AD can be classified according to the Stanford classification (LeMaire and Russel (2011)) as a Type A aortic dissection (TAAD) involving any part of the aorta proximal to the origin of the left subclavian artery or a Type B aortic dissection (TBAD), distal to the origin of the left subclavian artery. The diameters and volumes of the aorta, as well as its branches, the presence of mural thrombus, and the shape and area of the tears are crucial for properly characterizing AD (Rogers et al. (2011)). Pepe et al. (2020) recently discussed and reviewed the literature on AD.

An **intramural hematoma (IMH)** is a contained aortic wall hematoma with bleeding in the media without an intimal tear. Acute IMHs appear as focal, crescentic,

high-attenuating regions of eccentrically thickened aortic wall on non-contrast CT. IMH have a lower attenuation compared to the aortic lumen on post-contrast CT. IMH will displace atheromatous calcifications into the aortic lumen, while mural thrombus will displace calcifications away from the lumen. However, occasionally IMH, aortic thrombus and atherosclerotic thickening are difficult to distinguish with CT. In this case, MRI might be a better solution for diagnosis, as the method of dynamic cone gradient-echo sequences can be applied (Nienaber (2013)).

**Penetrating atherosclerotic ulcers** are ulcerating atherosclerotic lesions that penetrate the intima into the media of the aortic wall. (Bolger (2008)). In non-contrast CT images, PAU is similar to IMH. CTA is the preferred technique for the diagnosis of PAU, where the typical finding is a contrast filled out-pouching of the wall of the aorta or into a thickened aortic wall in absence of an intimal flap or false lumen, more commonly located in the descending aorta. The disadvantage of MRI is its limitation in displaying the displacement of the intimal calcifications, which can occur with PAU.

An **aortic aneurysm** is a focal or diffuse dilatation of the aorta involving all three layers of the aortic wall. It can be classified into thoracic aortic aneurysms (TAA) and abdominal aortic aneurysms (AAA). TAA can be detected in many locations on the thoracic aorta, and is, in most cases, asymptomatic. TAA is often detected when patients are examined with medical imaging for investigative reasons, which puts higher demands on the capabilities of medical imaging. AAA, as the name suggests, is detected in the abdominal aorta. With the improvement of technology, CT and MRI are now considered better than aortography and the current gold standard for diagnosis, as well as operative assessment of AAA. Diameter, length and curvature of the aorta are especially important for the surgical operation and repair of the aortic aneurysm (Erbel and Aboyans (2014)).

**Aortic atherosclerosis** is caused by endothelium activation and accumulation of lipids in the intimal and medial layers of the aortic wall (Hager et al. (2007)). The process of atherosclerosis can lead to many diseases, including thrombosis, atherosclerotic aortic occlusion, calcified aorta and coral reef aorta (Erbel and Aboyans (2014)). Imaging techniques (CT or MRI) are helpful in the diagnosis and treatment of atherosclerotic diseases by providing information about calcifications and plaques.

Furthermore, imaging techniques can be applied in the diagnosis and treatment of other aortic diseases, including traumatic aortic injuries, aortic coarctation, aortitis, connective tissue diseases such as Marfan and Loeys-Dietz syndromes, and more. They are also important for long-term follow-up and monitoring of aortic disease development. Non-invasive examinations help evaluate the conditions of patients and monitor treatment. Advanced segmentation methods can separate the aorta from other organs, and help the clinicians in analyzing the characteristics of patients and reach their diagnosis.

#### 4. Computer-aided Aortic Tree Segmentation

Based on our search, aortic vessel tree segmentation usually focuses on volume segmentation of healthy aortas in CT, CTA or MR images, while some studies also aim to segment specific aortic branches or aortas with different diseases. In this section, we introduced and compared various aorta segmentation algorithms from reviewed studies.

#### 4.1. Review Organization

Various aorta segmentation approaches were identified in this paper. In this subsection, we introduced the taxonomy of approaches and the performance metrics.

The approaches identified in this review can be roughly divided into four classes, namely, deformable models, tracking models, deep learning, and other techniques. We discuss these four classes in the following subsections. In addition, the pre-processing steps, the degree of automation, and the specific segmented parts of aortic vessel tree were also taken into account.

To compare the performance of different approaches from different studies, we mainly focused on their datasets and metrics. For datasets, we paid particular attention to data quality, namely the modalities and the amount of raw images, and the clinical status of patients. During our review, we found that research typically utilizes four methods for collecting the validation data. Most of them obtained the raw medical images from retrospective examinations of hospitals or other specific healthcare facilities, while others also considered publicly available datasets or relied on synthetic images or digital phantoms. Only a few studies prospectively recruited volunteers or patient data for validation.

Different metrics have been proposed for performance evaluation: time taken to complete a segmentation and the accuracy of segmentation results against the standard of practice were most common. Researchers have applied several qualitative and quantitative metrics of segmentation accuracy. In earlier times, the approaches were usually evaluated visually. The researchers invited clinical experts to manually evaluate their segmentation results and/or give a score of segmentation performance. In some studies, researchers might only give examples to show their segmentation results, which makes it difficult to compare the segmentation results with other studies.

Then a metric called volume error (VE) was sometimes applied based on:

$$VE = \frac{|V(A) - V(B)|}{V(A)} \quad (1)$$

where  $V(A)$  and  $V(B)$  are volumes of original and correctly classified images, respectively. This metric can partly represent the segmentation performance, but has problems when a small object is segmented from a relative large background.

In recent years, more studies have applied another metric called the dice similarity coefficient (DSC) (Taha and Hanbury (2015)), which can be defined as:

$$DSC = \frac{2|A \cap B|}{|A| + |B|} \quad (2)$$

where  $|A|$  and  $|B|$  represent the voxels of aortic vessels in segmentation and ground truth images, respectively. It is essentially a measure of overlap between two sets and can better evaluate the segmentation approaches.

In addition, the Hausdorff distance (HD), which measures the local maximum distance between two surfaces, is also applied to evaluate the segmentation performance. It can be defined as:

$$HD = \max\{\sup_{s \in S} \inf_{g \in G} d(s, g), \sup_{g \in G} \inf_{s \in S} d(s, g)\} \quad (3)$$

where  $S$  and  $G$  are the segmentation results and the ground truth,  $d$  represents the Euclidean distance,  $sup$  is the supremum and  $inf$  is the infimum.

One additional metric called average symmetric distance (ASD) can also help during the evaluation (Heimann et al. (2009)). It is defined as:

$$ASD = \frac{1}{|P(A)| + |P(B)|} \left( \sum_{P(A)} d(P_A, P(B)) + \sum_{P(B)} d(P_B, P(A)) \right) \quad (4)$$

where  $P(A)$  and  $P(B)$  are the set of points from region A and B;  $d(P_A, P(B))$  and  $d(P_B, P(A))$  are the shortest distances between any point from region A to region B and vice versa, calculated with the Euclidean distance.

#### 4.2. Deformable Models

Deformable models (Kass et al. (1988), Terzopoulos and Metaxas (1991)) apply curves or surfaces to move and fit the contours of images. The goal of the fitting process is usually to minimize an energy function influenced by external and internal forces. External forces pull the curves or surfaces towards the contours, while internal forces are designed to resist deformation and therefore ensure smooth results. Deformable model approaches can further be classified into edge-based and region-based approaches.

As one of the most widely used segmentation algorithms in the early stages, studies based on deformable model algorithms have a long time span. In 1997, Rueckert et al. (1997) published their research on aorta segmentation based on a deformable model approach. The authors presented a novel algorithm for the tracking of the aorta in cardiovascular MR images. A multiscale medial response function was first applied to roughly locate the aorta. This estimate was then refined with a deformable model, which was defined in a Markov-Random-Field framework. The results have been evaluated with clinical compliance studies to show its ability in clinical applications.

Krissian et al. (2014) proposed to use a combination of methods to segment aortas affected by AD. They first applied pre-processing methods to remove image noise and other organs from original images. Then, a multiscale algorithm was applied to extract the possible centerlines. Additional centerlines (false positives) could be present due to smaller vessels or bones missed during the pre-processing step and therefore a manual centerline selection step was always performed. Finally, the selected centerlines were used as initialization points to extract the aortic wall as well as the AD flap with a level-set algorithm. The workflow is shown in Figure 4. This approach was evaluated with synthetic and real images from three patients with AD. The authors compared the segmentation results of their approach with manually segmented dissections. The comparison showed an average distance of about 0.5 voxels. However, the lack of data still posed difficulties in making a convincing assessment. Some steps of the complicated pre-processing and manual extraction of centerlines should also be simplified.

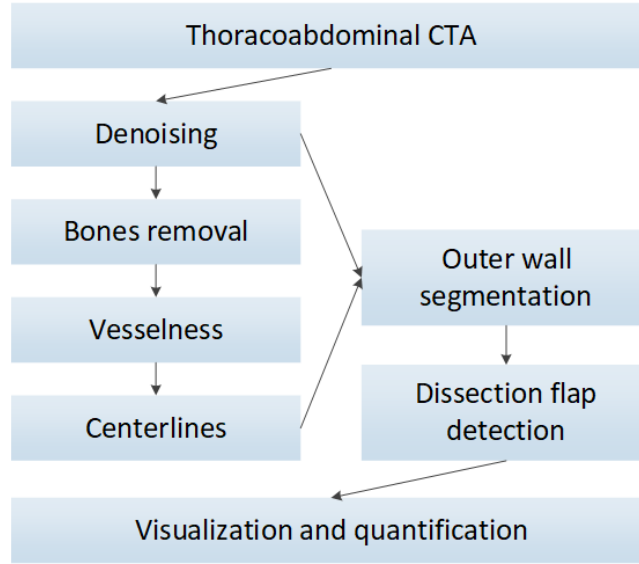


Figure 4: Workflow of aorta segmentation in Krissian et al. (2014). CTA: computed tomography angiography.

Kurugol et al. (2015) proposed a 3D level-set method to segment the aorta in CT images and performed calcification detection. Aorta segmentation was based on a selected region of interest from the original images. The initialization of the aortic surface was based on its approximate tubular shape. At first, a rough surface was created slice by slice within two steps: (1) A circular Hough transform was applied to detect circles slice by slice; (2) the contour of the aorta was selected from all the detected circles based on the posterior probability related to the Hough transform, the spatial smoothness prior and the current slice. Then, a refinement of all the selected aortic circles was performed based on a 3D level-set method, which evolves the shape of the initialized surface to match the real aortic edge. In addition to the segmentation of the aortic wall, they also attempted an automatic detection of calcifications by using a simple threshold-based method to segment plaques with more than 130 Hounsfield units (HU). However, the method has some limitations, including application range and segmentation accuracy. Some of the segmented calcification plaques were actually healthy aortic wall, which is usually located in regions of high HU values. In addition, this method can only be applied to specific CT images with stable HU values, and the threshold value needs to be tuned for different images to get better segmentation results.

Deformable model approaches are widely applied in the field of vessel segmentation (Moccia et al. (2018)). One limitation of these algorithms is that deformable models are mainly driven by external forces of image densities. As a result, it is challenging to segment the aorta from original images which have weak intensity gradients or image noise. In addition, the deformable model approaches usually need to be initialized, which means few studies have applied deformable model algorithms to perform a fully

automatic segmentation of the aorta.

A summary of the deformable model algorithms is presented in Table 3. From this table, the main advantage of deformable model algorithms is their directness. In the past decades, when insufficient computing resources were available, deformable models could still be applied to segmentation tasks on common hardware. Additionally, this algorithm does not have large requirements for ground truth information, so it's still usable with less data support. However, this type of segmentation algorithm demands stronger contrast within original images. Therefore, all segmentation tasks based on deformable algorithms were achieved after many relatively complex pre-processing steps. Moreover, in these algorithms, the gradient of boundary pixels (voxels) is repeatedly calculated, which means this type of algorithm cannot be directly applied to the original medical images. To resolve it, some studies used prior knowledge of medical imaging to remove other organs and improve image quality (Zhuge et al. (2006), Lareyre et al. (2019)). Others chose to manually select the regions of interest to improve segmentation efficiency and reduce errors. Despite these problems, the deformable model algorithms are still widely applied as unsupervised or semi-supervised segmentation methods, especially when they are used mainly for segmentation refinement.



Table 3: Summary of deformable model algorithms for aorta segmentation. Note that the number of digits after the decimal points vary, because we used the original numbers provided within the publications.

Study	Algorithm	Method			Modality	Dataset No.	Disease	Duration	Evaluation		
		Pre.	Auto	SVT					RS	Metrics	Statistic
Rueckert et al. (1997)	EM	A	=	=	MRI	87(p)	-	3min	GT	VE	2.21
Loncaric et al. (2000)	LS	R	-	=	CTA	1(p)	AAA	NA	OB	-	-
Olabarriaga et al. (2005)	GLM	R	=	=	CTA	17(p)	AAA	41s	GT	VE/MDE	4.5/1.3
Das et al. (2006)	AC	D&M	=	=	CT	7(d)	AAA	NA	GT	DSC	>85.1
Zhuge et al. (2006)	LS	D	+	=	CTA	20(p)	AAA	7min	GT&C	VE/MDE	3.5/0.6
Herment et al. (2010)	DM	R&A	-	=	PCMR	52(p&v)	-	17s	GT&C	DSC	94.5
Auer and Gasser (2010)	DM	R	-	=	CTA	11(p)	AAA	NA	C	MDE	-
Krissian et al. (2014)	AC	D	-	+	CT	3(s)/5(p)	-/AD	8min	OB&C	MDE	-
Kurugol et al. (2015)	LS	R	-	-	CT	45(d)	AC	NA	GT	DSC	92
Volonghi et al. (2016)	LS	D&R	-	+	PCMR	6(v)	-	30s	GT	MDE/DSC	<1.44/>88
Gao et al. (2016)	DM	D	+	+	CTA	36(p)	-	90s	GT&C	DSC	>95
Duan et al. (2016)	GVF	M	=	+	CT	5(p)	AD	1s	GT	DSC	92.7
Morais et al. (2017)	BEAS	R	-	=	CT	42(p)	d	73s	GT	DSC/HD	94/1.61
Wang et al. (2017)	AC	D&M	=	=	CEMRA	19(p)	AAA	35s	GT&C	DSC	89.8
Bidhult et al. (2019)	AC	M&R	-	=	PCMR	191(p&v)	-	<3.1s	GT	DSC	95.3
Lareyre et al. (2019)	AC	D&A	+	=	CT	40(p)	AAA	<1min	GT	DSC/HD	93/1.78
Zhao et al. (2022)	MSMR	A	+	=	CTA	35(d)	AD	16.6s	GT&C	DSC/HD	94.12/2.85

List of abbreviations:

Algorithm: EM = energy minimizing, LS = level set, GLM = grey level model, AC = active contour, DM = deformable model, GVF = gradient vector flow, BEAS = B-spline explicit active surfaces, MSMR = morphology-constrained stepwise deep mesh regression.

Pre-processing before main segmentation process (Pre.): M = manual segmentation of contours, A = (semi) automatic delineation of contours, R = region of interest or start point selection, D = denoising or bone removal, (-) not mentioned.

Automation according to the whole segmentation process (Auto): (+) fully automatic, (-) semi-automatic, (=) more manual guidance required. Initialization steps that go beyond parameter setting and region of interest or start point selection are also defined as excess manual guidance.

Segmented parts of aortic vessel tree (SVT): (+) whole aorta with/without some of its branches, (-) thoracic aorta with/without some of its branches, (=) only part of thoracic aorta. According to Figure 1 and Table 1, whole aorta refers to aortic parts 1-4 and thoracic aorta refers to aortic parts 1-3.

Modality: MRI = magnetic resonance imaging, CTA = computed tomography angiography, CT = computed tomography, PCMR = phase-contrast magnetic resonance, CMR = cardiovascular magnetic resonance, CEMRA = contrast enhanced magnetic resonance angiography.

Number of data for method validation (No.): p = patients from specific health facilities, d = data from public datasets or challenges, v = volunteers, s = synthetic images.

Aortic diseases: (-) no disease, d = different diseases, AAA = abdominal aortic aneurysm, AD = aortic dissection, AC = aortic calcification.

Duration: NA = not available / reported, min = minute, s = second.

Reference standard (RS): GT = ground truth, OB = human observer, C = comparison with other approaches or literature.

Metrics: VE = volume error (%), DSC = dice similarity coefficient (%), MDE = mean distance error (mm), HD = Hausdorff distance (mm).

### 4.3. Tracking Models

Tracking approaches usually start from a set of initial seed points and use specific growth algorithms to track the vessels and iteratively select new candidate vessel points. Seed points are either manually selected or automatically defined. Although tracking approaches are widely used in the field of vessel tree segmentation (Robben et al. (2014); Chen et al. (2016); Biesdorf et al. (2015); Wang et al. (2012); Lee et al. (2017)), most of their applications focus on vessel trees of the brain, retinal vessels or coronary arteries. There are fewer studies which apply tracking algorithms to segment the aortic tree.

Subramanyan et al. (2003) were among the first to employ tracking approaches for aorta segmentation. The authors proposed a semi-automatic method to track the aortic vessel tree from selected seed points. The fast marching method (Sethian and Vladimirsky (2000)) was applied to delineate the blood flow, and the distance transform method was then used to extract centerlines. Finally, the fast marching method was reinitialized in a blood filled region, and the CT volume was subtracted to obtain the contours of the aortic thrombus. This approach was evaluated simply using spatial localization and diameter determination compared with manual and 3D volume rendering methods.

Biesdorf et al. (2011) proposed a model-based tracking method for aorta segmentation and analysis in dynamic 4D electrocardiogram gated computed tomography angiography (ECG-CTA) images. Firstly, a 3D model of the vessels was created based on the parameters of the vessel width, image blur and voxel position. A coarse aorta segmentation was then performed through a gradual fitting process, which was manually initialized by the vessel model. The segmentation was then refined using a Kalman filter and the vessel model. Finally, the 3D motion of the aorta was determined with intensity-based matching. The authors evaluated their method based on Euclidean distance between manually obtained and method-based centerline positions and vessel diameters. However, these two parameters cannot fully represent the segmentation results, as they assume that the aorta is circular along its centerline.

Martínez-Mera et al. (2013) proposed to segment the thoracic aorta in CTA images using a combination of level-set and region growing algorithms. As shown in Figure 5, two methods were applied, respectively, to segment the aorta in this study. Parts of the whole aortic tree (partial ascending aorta, aortic arch, descending aorta and some aortic branches) were segmented based on a region growing algorithm. The Hough transform was applied to locate the aorta in the original image and initialize the seed points. Regions were then grown based on the mean and variance of neighboring voxels. The other part of the ascending aorta was then segmented with a level-set algorithm. These two parts were combined to reconstruct the whole aorta. They evaluated their method on ten different CT images and achieved a mean DSC of 0.943 and a Pearson's correlation coefficient (PCC) of 0.972. However, image noise easily affects this method, as the main part of the aorta is segmented by a simple neighbourhood-based region growing algorithm. The combination of segmentation results based on two different methods may also cause incoherence in the connecting surface.

Among current studies on aorta segmentation, the tracking approaches have required the highest continuity in the original images. In this case, the noise in medical

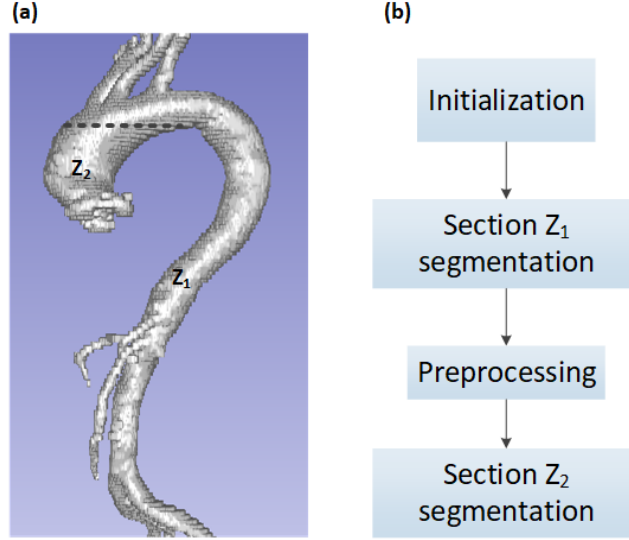


Figure 5: (a) Two parts ( $Z_1$  and  $Z_2$ ) of the aorta were segmented respectively with the method of Martínez-Mera et al. (2013) (dataset courtesy: Dongyang Hospital). (b) Workflow of the proposed method for aorta segmentation. Section  $Z_1$  was first segmented applying a region growing algorithm, then section  $Z_2$  was segmented with a level-set algorithm.

images can have a significant impact on the segmentation results. Different approaches, including region growing algorithms, model-based algorithms, ellipse estimation algorithms, and many others, have been applied to track the aortic vessel tree. More algorithms, such as particle filter algorithm (Lee et al. (2017)) and statistical Bayesian algorithm (Wang et al. (2012)), have been used to track other blood vessels and could potentially be extended to the field of aortic tree segmentation.

A summary of the current studies on tracking algorithms can be found in Table 4. Similar to deformable model algorithms, tracking algorithms can also be applied as unsupervised or semi-supervised segmentation methods. The core difference is that in tracking algorithms the most attention is paid to image continuity (contours or center lines). In addition, the segmentation process of tracking algorithms is usually faster and easier to visualize. However, these algorithms require even higher image quality than the deformable methods. Thin blood vessels are more likely to be ignored. If the segmentation target is the entire aortic vessel tree, a refinement process should be required after the tracking process.

Table 4: Summary of tracking algorithms for aorta segmentation. Note that decimal precision varies, as we report the original numbers provided within the original studies.

Study	Algorithm	Method			Modality	Dataset No.	Disease	Duration	Evaluation		Statistic
		Pre.	Auto	SVT					RS	Metrics	
Subramanyan et al. (2003)	FM	R	-	-	CT	15(p)	AT	<90s	C	-	-
Boskamp et al. (2004)	RG	R	-	=	CTA	1(p)	-	NA	OB	-	-
Zheng et al. (2010)	PB	-	+	-	CBCT	192(d)	-	1.4s	GT	SPD	1.1
Biesdorf et al. (2011)	MB	R&A	-	-	ECG-CTA	30(p)	-	NA	GT	CP	1.53
Egger et al. (2009)	GB	R&M/A	=	-	CTA	50(p)	AT	<90s	GT	DSC	90.67
Martínez-Mera et al. (2013)	RG&LS	A	+	+	CTA	10(p)	-	NA	GT	PCC	93.83
Xie et al. (2014)	MB	R	-	-	CT	359(d)	-	NA	GT&C	DSC/MDE	93.3/1.39
Selver and Kavur (2016)	3D-PGDF	R	-	=	CTA	19(d)	AAA	80.3s	GT&C	DSC/MDE	71.07/0.31
Tahoces et al. (2019)	ET	-	+	-	CT	380(d)	d	NA	GT	DSC/MDE	95.1/0.9

List of abbreviations:

Algorithm: FM = fast marching, RG = region growing, PB = part-based tracking, MB = model-based tracking, GB = graph-based tracking, LS = level set, 3D-PGDF = 3D pairwise geodesic distance field, ET = ellipse tracking.

Pre-processing before main segmentation process (Pre.): M = manual segmentation of contours, A = (semi) automatic delineation of contours, R = region of interest or start point selection, D = denoising or bone removal, (-) not mentioned.

Automation according to the whole segmentation process (Auto): (+) fully automatic, (-) semi-automatic, (=) more manual guidance required. Initialization steps that go beyond parameter setting and region of interest or start point selection are also defined as excess manual guidance.

Segmented parts of aortic vessel tree (SVT): (+) whole aorta with/without some of its branches, (-) thoracic aorta with/without some of its branches, (=) only part of thoracic aorta. According to Figure 1 and Table 1, whole aorta refers to aortic parts 1-4 and thoracic aorta refers to aortic parts 1-3.

Modality: CT = computed tomography, CTA = computed tomography angiography, CBCT = cone beam computed tomography, ECG-CTA = electro-cardiogram gated computed tomography angiography.

Number of data for method validation (No.): p = patients from specific health facilities, d = data from public datasets or challenges, v = volunteers, s = synthetic images.

Aortic diseases: (-) no disease, d = different diseases, AAA = abdominal aortic aneurysm, AT = aortic thrombus.

Duration: NA = not available / reported, min = minute, s = second.

Reference standard (RS): GT = ground truth, OB = human observer, C = comparison with other approaches or literature.

Metrics: SPD = symmetric point-to-mesh distance (mm), CP = mean error of centerline position (mm), DSC = dice similarity coefficient (%), PCC = Pearson's correlation coefficient (&), MDE = mean distance error (mm).

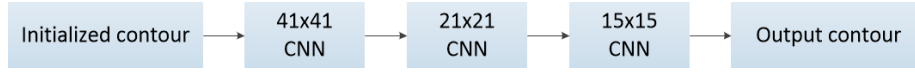


Figure 6: Structure of the proposed cascaded convolutional neural networks (CNNs) for aorta segmentation in Li et al. (2019). Three similar 2D CNN structures with different kernel sizes are applied.

#### 4.4. Deep Learning

Long et al. (2014), Ronneberger et al. (2015) and Çiçek et al. (2016) were among the first successful works on medical image segmentation with deep learning. Deep learning approaches have been widely used for the task of medical image segmentation ever since (Hesamian et al. (2019)). In this survey, deep learning approaches refer to methods that use training data with their respective labeled ground truth to train a convolutional neural network in a supervised manner.

Deep learning methods are used to extract meaningful features directly from the original data and infer the expected segmentation labels. Thanks to the wide availability of open-source code and libraries, the main advantage of deep learning in medical imaging is its straightforward application for segmentation tasks without tedious manual operations. However, the training of a deep learning model requires a large amount of labelled data, which is often not available in medical imaging. Furthermore, 3D medical images usually come with high resolutions and can often not be directly fed to deep networks due to limited computational resources. As a result, pre-processing steps and patch-based training, e.g. for aortic landmarking (Codari et al. (2020); Schmied et al. (2021)), are often used to cope with hardware limitations (Litjens et al. (2017)).

To our knowledge, Trullo et al. (2017) were the first to apply a deep learning approach for aorta segmentation. The authors used fully convolutional neural networks (FCN) to segment four different human organs, including the aorta, in CT imaging. The authors additionally evaluated two approaches to refine the FCN results: the conditional random fields (CRF) and the SharpMask (SM) architecture (Pinheiro et al. (2016)). With a dice score of 0.86, their evaluation showed that the combination of SM and CRF achieved the best accuracy for aorta segmentation.

Two years later, Li et al. (2019) proposed a cascaded convolutional neural network (CNN) to segment the two aortic lumens in CT scans from patients with AD. The authors first manually extracted 2D cross sections along the aortic centerlines using the Visualization Toolkit (VTK) [<https://vtk.org/>]. An aortic contour was initialized as an ROI (region of interest) in each cross section. Then, a structure of cascaded 2D CNNs, as shown in Figure 6, was applied to segment the intima as well as adventitia contours within the ROI. Finally, the segmentation results were reconstructed into 3D volumes using the VTK.

Fantazzini et al. (2020) proposed a combination of several CNNs to overcome the problem of high resolution image segmentation. The workflow is shown in Figure 7. First, the original images were downsampled, so they could be inputted into a 3D CNN to obtain an aorta segmentation. These results were mainly used as a rough location of the aorta in the original images, and a volume of interest could be cropped. Then, three 2D CNNs were applied to segment the aorta from the cropped volumes in order to perform 2D segmentations based on axial, sagittal and coronal views, respectively. An

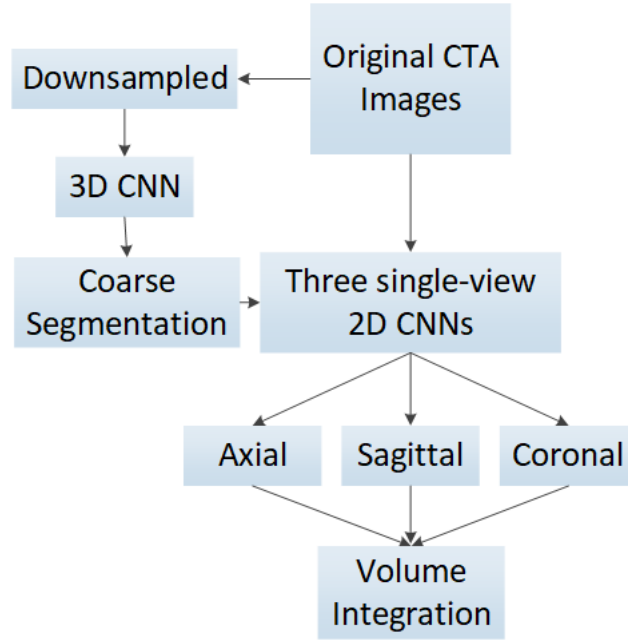


Figure 7: Workflow of the proposed method for aorta segmentation in Fantazzini et al. (2020). A 3D CNN (convolutional neural network) is first used to locate the aorta and three 2D CNNs are then applied to segment the aorta under high resolution based on axial, sagittal and coronal views. An aortic volume segmentation is performed with the integration of these three views. CTA: computed tomography angiography.

aortic volume segmentation was performed with the integration of these three views.

Currently there are still relatively few studies that apply deep learning algorithms to segment the aorta. The main reason may be due to the lack of labelled datasets, like Radl et al. (2022a,b), which has recently been released. The training and evaluation of a deep neural network requires enough training data with ground truth labels. This introduced a strong requirement for manual work of domain experts, like radiologists. In addition, ground truth labels created by different experts may also show a non-negligible inter-operator variability (Litjens et al. (2017)). Detailed subdivision of different parts of the aorta and its branches, as shown in Figure 1, during the manual annotation, could improve the universality of datasets.

A summary of the current studies about deep learning algorithms is presented in Table 5. These deep learning-based approaches have only become popular in recent years, but have shown high potential (Shen et al. (2017)). Compared with the previous two methods, deep learning-based approaches are often fully automatic. End users can simply provide the original medical images as input and obtain a segmentation without manual initialization or selection of seed points. A well trained deep learning model can directly output the segmentation results. In addition, it can be applied as a pixel-wise segmentation method to segment thin blood vessels and be utilized with medical images with a lot of noise. However, as a supervised learning algorithm, a well-trained

deep learning model typically requires a large set of original images with ground-truth masks. It makes data collection and processing the main challenge of deep learning approaches (Shen et al. (2017); Pepe et al. (2020)).

Table 5: Summary of deep learning algorithms for aorta segmentation. Note that the number of digits after the decimal points vary, because we used the original numbers provided within the publications.

Study	Algorithm	Method Pre.	Auto	SVT	Modality	Dataset		Disease	Duration	Evaluation		
						No.				RS	Metrics	Statistic
Trullo et al. (2017)	SM&CRF	N	+	-	CT	30(p)		-	NA	GT	DSC	86
López-Linares et al. (2018)	HED	-	+	=	CTA	13(p)		AT	NA	GT&C	DSC	82
Cao et al. (2019)	3D U-Net	N&Aug	+	-	CTA	276(p)		AD	31.1s	GT	DSC	93
Fantazzini et al. (2020)	U-Net	N&R&Aug	+	+	CTA	80(p)		AAA	25s	GT	DSC	93
Howard et al. (2020)	HRNet	N	+	-	CMR	575(p)		-	NA	GT	DSC	92.9
Berhane et al. (2020)	3D U-Net	N&D	+	-	4D flow MRI	1193(p)		-	0.44s	GT	DSC/HD	95.1/2.8
Hahn et al. (2020)	TernausNet	-	+	-	CT	153(p)		AD	<4min	GT	DSC	94.9
Chen et al. (2021)	DenseNet	N	-	+	CT	120(p)		AD	14.2s	GT	DSC	97
Yu et al. (2021)	3D U-Net	R&D	-	+	CTA	139(p)		AD	21.7min	GT	DSC	95.8
Jin et al. (2021)	V-Net & PF	Aug	+	-	CT & CTA	80(d)		-	NA	GT&OB	VE	<0.255
Zhong et al. (2021)	AG U-Net	N&P	+	-	CTA	194(p)		-	NA	GT	DSC	96.6
Sieren et al. (2022)	3D U-Net	-	+	=	CTA	191(p)		d	60.5s	GT	DSC	95

List of abbreviations:

Algorithm: SM = Sharp Mask, CRF = Conditional Random Fields, HED = Holistically-Nested Edge Detection, HRNet = High Resolution Net, PF = Particle Filter, AG U-Net = Attention-Gated U-Net.

Pre-processing before main segmentation process (Pre.): R = region of interest or start point selection, Aug = data augmentation, N = normalization of data (value and size), A = (semi) automatic delineation of contours, R = region of interest or start point selection, P = patches division, D = denoising or bone removal, (-) not mentioned.

Automation according to the whole segmentation process (Auto): (+) fully automatic, (-) semi-automatic, (=) more manual guidance required. Initialization steps that go beyond parameter setting and region of interest or start point selection are also defined as excess manual guidance.

Segmented parts of aortic vessel tree (SVT): (+) whole aorta with/without some of its branches, (-) thoracic aorta with/without some of its branches, (=) only part of thoracic aorta. According to Figure 1 and Table 1, whole aorta refers to aortic parts 1-4 and thoracic aorta refers to aortic parts 1-3.

Modality: CT = computed tomography, CTA = computed tomography angiography, CMR = Cardiovascular magnetic resonance, CBCT = cone beam computed tomography, ECG-CTA = electro-cardiogram gated computed tomography angiography.

Number of data for method validation (No.): p = patients from specific health facilities, d = data from public datasets or challenges, v = volunteers, s = synthetic images.

Aortic diseases: (-) no disease, d = different diseases, AT = aortic thrombus, AD = aortic dissection, AAA = abdominal aortic aneurysm.

Duration: NA = not available / reported, min = minute, s = second.

Reference standard (RS): GT = ground truth, OB = human observer, C = comparison with other approaches or literature.

Metrics: DSC = dice similarity coefficient (%), HD = Hausdorff distance (mm), VE = volume error(%).



#### 4.5. Other Techniques

In addition to the three main categories, some studies applied other algorithms for aorta segmentation tasks, although less frequently. Due to the relatively small number of studies based on similar algorithms, these approaches are introduced in this additional subsection.

de Bruijne et al. (2002) presented an automatic method based on active shape models (ASM). They applied this method to segment thrombus regions in CTA images of abdominal aortic aneurysms. The original ASM approach was improved with a  $k$  nearest neighbour ( $k$ NN) method, which was used to obtain the probability density estimation that any given profile belongs to the aortic boundary. The comparison of segmentation results of both the original and the improved ASM method showed that the introduction of  $k$ NN significantly reduced the leave-one-out error from 2.2 to 1.6 mm.

Duquette et al. (2012) applied a graph cut algorithm to segment the aortic volume (Boykov et al. (2001)) in 3D CT and MR images. This method can also be seen as an assistance to manual segmentation: The users roughly select the aortic contour in several slices of the 3D images. As shown by Figure 8, the original volume would be divided into three sections: inner section, neutral section, and outer section. Voxels in the inner section (blue) are all connected to the source, while voxels of outer section (green) are all connected to the sink. The graph cut algorithm deals with the voxels in the neutral section (red) to perform an accurate segmentation. An edge capacity of two neighbouring voxels  $a$  and  $b$  is calculated with:

$$Capacity = \exp\left(-\frac{f_{ab}|I_a - I_b|^\gamma}{2\sigma^2}\right), \quad (5)$$

where  $I$  is the voxel intensity,  $\gamma$  is a parameter for gradient-based gamma correction, and  $f$  is a binary function, which prevents the segmentation of edges of neighbouring organs. This equation takes into account the gradient information to suit different voxel densities/intensities of CT and MR images. In areas with stronger gradients, the connections between voxels were cut to generate the contours. A manual refinement step usually followed the graph cut method. The authors compared their method against manual segmentations performed by four domain experts. Their comparison showed that the results are sufficiently comparable to the ground truth, which led them to the conclusion that the method can be applied to computer-assisted manual segmentation. An automatic or semi-automatic application of this algorithm can also be realized.

In Gamechi et al. (2019), a combination of imaging techniques was applied to segment the aorta in CT images. At first, pre-processing was used to remove the heart, lung and bones from the original CT images. Then, the authors used a multi-atlas-based method (Kirişli (2010)) to coarsely locate the aorta. The preprocessed images were registered to the target model, and ten of them were selected for the following approaches. Aortic centerlines were traced based on the minimum cost path algorithm. Finally, a graph cut segmentation algorithm was applied to accurately segment the aortic surface based on the traced centerlines. The segmentation results were evaluated based on 100 CT images with manually segmented ground truths. This approach has achieved an average DSC of  $0.95 \pm 0.01$  and a MSD of  $0.56 \pm 0.08$  mm.

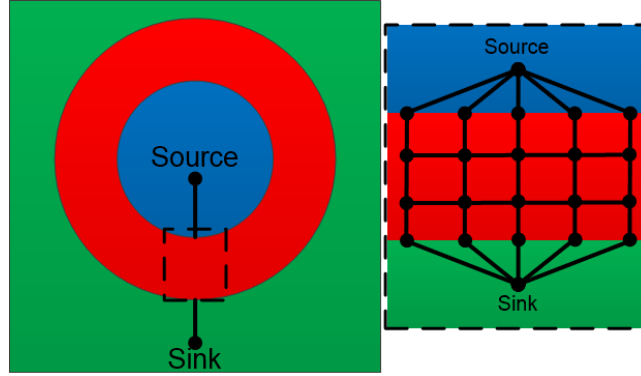


Figure 8: Schematic representation of an initialized aortic area (Duquette et al. (2012)). Voxels inside the blue area are all connected to the source, and those in green are connected to the sink. Voxels in the middle (red) are connected to their six neighbouring voxels.

There are several algorithms applied to segment vessels, but not yet specifically used in semantic aorta segmentation. Li et al. (2006) developed an optimal surface detection method to detect multiple interacting surfaces, which was applied to segmentation tasks on more than 300 computer-generated 3D images. Egger et al. (2007) proposed a fast vessel centerline extraction method, which can also be applied for aorta segmentation tasks. Bruyninckx et al. (2010) applied a global optimization algorithm to segment liver portal veins in CT images. Sreejini and Govindan (2015) applied a particle swarm optimization algorithm to segment retinal vessels. Tang et al. (2012) used a minimum cost path algorithm to segment carotids in MRI. These segmentation algorithms could potentially be extended to the field of aortic vessel tree segmentation.

A summary of additional algorithms is presented in Table 6.

Table 6: Summary of additional algorithms for aorta segmentation. Note that the number of digits after the decimal points vary, because we used the original numbers provided within the publications.

Study	Algorithm	Method			Modality	Dataset No.	Disease	Duration	Evaluation		
		Pre.	Auto	SVT					RS	Metrics	Statistic
de Bruijne et al. (2003)	ASM	A	-	=	CTA	23(p)	AAA	25s	C	VE	5.9
Bodur et al. (2007)	IA	R	-	-	CTA	4(P)	AAA	10min	OB	-	-
Duquette et al. (2012)	GC	R	-	=	CT& MRI	44(p)	AAA	<1min	GT	HD	<3.53
Freiman et al. (2012)	WS	D	-	=	CTA	56(d)&15(p)	-	122s	GT&C	DSC	84.5
Bustamante et al. (2015)	AM	-	+	+	CMR	11(v)/10(p)	-/d	NA	OB	-	-
Gamechi et al. (2019)	MR	-	+	-	CT	16(p)	-	NA	GT	DSC	95

List of abbreviations:

Algorithm: ASM = Active Shape Models, IA = Isoperimetric algorithm, GC = Graph Cut theory, WS = Watershed-based segmentatoin, AM = atlas-based model, MR = Multi-atlas registration.

Pre-processing before main segmentation process (Pre.): R = region of interest or start point selection, Aug = data augmentation, N = normalization of data (value and size), A = (semi) automatic delineation of contours, R = region of interest or start point selection, P = patches division, D = denoising or bone removal, (-) not mentioned.

Automation according to the whole segmentation process (Auto): (+) fully automatic, (-) semi-automatic, (=) more manual guidance required. Initialization steps that go beyond parameter setting and region of interest or start point selection are also defined as excess manual guidance.

Segmented parts of aortic vessel tree (SVT): (+) whole aorta with/without some of its branches, (-) thoracic aorta with/without some of its branches, (=) only part of thoracic aorta. According to Figure 1 and Table 1, whole aorta refers to aortic parts 1-4 and thoracic aorta refers to aortic parts 1-3.

Modality: CT = computed tomography, CTA = computed tomography angiography, CMR = Cardiovascular magnetic resonance, CBCT = cone beam computed tomography, ECG-CTA = electrocardiogram gated computed tomography angiography.

Number of data for method validation (No.): p = patients from specific health facilities, d = data from public datasets or challenges, v = volunteers, s = synthetic images.

Aortic diseases: (-) no disease, d = different diseases, AT = aortic thrombus, AD = aortic dissection, AAA = abdominal aortic aneurysm.

Duration: NA = not available / reported, min = minute, s = second.

Reference standard (RS): GT = ground truth, OB = human observer, C = comparison with other approaches or literature.

Metrics: DSC = dice similarity coefficient (%), HD = Hausdorff distance (mm), VE = volume error(%).

## 5. Clinical Application

In section 4, we described the main algorithms applied to segment the aorta in medical images. In this section, we introduce some studies on the clinical applications of these approaches, which usually include aortic disease detection (AD, calcification, etc.) and measurement of aortic parameters (diameter, volume, etc.).

An approach for aorta segmentation in CT images, proposed by Gamechi et al. (2019), was introduced in subsection 4.5. The authors introduced a different application of the proposed segmentation method. As shown in Figure 9, aortic diameter measurements were extracted from multiple cross-sectional slices from segmentation results. Evaluation has shown a small error between automatically and manually obtained aortic diameters, which means this automatic approach can support the clinical analysis of aortas based on original CT images.<sup>2</sup>

Krissian et al. (2014) proposed a method to perform aorta segmentation in CTA images of ADs. This method was developed to segment the dissection flap and support clinicians with the detection and analysis of ADs.

Bidhult et al. (2019) proposed an approach based on the active contour algorithm to segment vessel volumes from phase-contrast magnetic resonance images. The method was initialized on manually selected vessels of interest, followed by steps of automatic modification, as shown in Figure 10. This method was evaluated with 151 human aortas and showed an average DSC of 0.953. In the same study, the algorithm was also applied to measure the blood flow volume and quantify the shunt volume, which demonstrated its clinical applicability.

Auer and Gasser (2010) proposed a method based on snake models to segment a part of the human aorta, followed by additional steps for finite element mesh generation. Erhart et al. (2015) applied this method to perform finite element analysis (FEA) on different kinds of abdominal aortic aneurysms. The geometrical parameters of aortic diameters and volumes were obtained from the segmented aorta, and the mechanical parameters of Peak Wall Stress (PWS), Peak Wall Rupture Index (PWRI) and Rupture Risk Equivalent Diameter (RRED) were calculated based on the homogeneous model properties of wall thickness, mesh size and connective tissue characterization. FEA was performed on different datasets of asymptomatic, symptomatic and ruptured AAAs and the results were compared to support the clinical detection and analysis of AAA.

## 6. Conclusion and Discussion

In this review, we presented a summary of the literature for aortic vessel tree segmentation. We introduced the main aortic pathologies, as well as their clinical treatments, to show the importance of medical imaging techniques for the detection and analysis of aortic diseases. Then, we listed studies of aortic vessel tree segmentation

---

<sup>2</sup>Egger et al. (2007, 2012) also extracted aortic diameter measurements for minimally invasive stent planning and Li et al. (2018) extracted aortic diameters in aortic dissections, like the true and false lumens, and the length of the proximal landing zone for treatment planning.

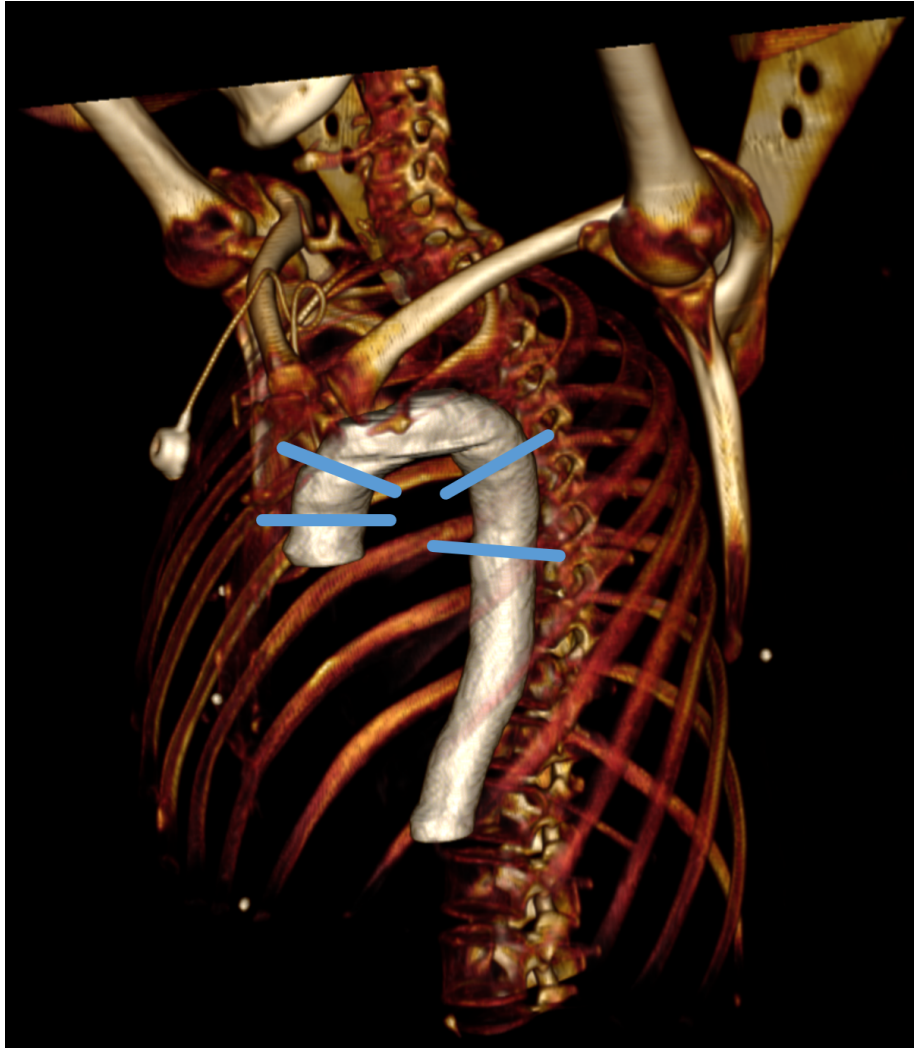


Figure 9: Aorta segmentation results (SegTHOR database (Trullo et al. (2017))), were used by Gamechi et al. (2019) to measure aortic diameters at different aortic points (blue lines, image rendered with InVesalius (Amorim et al. (2015))).

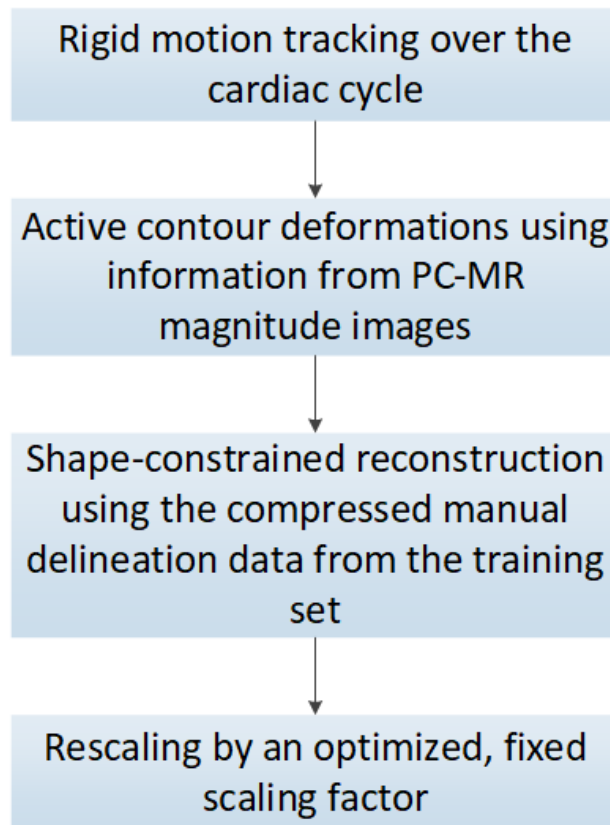


Figure 10: Workflow of the automatic modification of the method in Bidhult et al. (2019). PC-MR: phase-contrast magnetic resonance.

and classified them into four categories: deformable model approaches, tracking approaches, deep learning approaches and additional approaches. The advantages and disadvantages of these approaches were analyzed. In addition, we introduced algorithms that were applied for segmentation tasks of other human vessels, but were not yet used to segment the aorta. Possible applications of segmented aortic volumes were described to give these segmentation approaches more clinical significance.

### *6.1. Current State*

Based on our analysis, the distribution of different algorithm categories has changed over time. In the last three years, more studies have applied deep learning approaches to aorta segmentation tasks, while before, more studies applied deformable model and tracking approaches.

Deformable model and tracking algorithms usually involve multiple steps to automatically or semi-automatically segment aortas or aortic branches from original medical images. These approaches have no requirements for large amounts of data, although annotated datasets are still needed for the evaluation. Each study may segment different parts of aorta, which poses a problem when evaluating and comparing different approaches.

With the development of deep learning algorithms, as well as the increasing number of datasets relating to the aorta, deep learning approaches have played a more significant role in the field of aorta segmentation tasks in recent years. The main advantages of deep learning approaches are the fully-automatic process and its pixel-wise segmentation performance, which makes it very straightforward to obtain segmentation results. However, a well-trained deep learning model needs a large amount of training data, which is relatively hard to obtain in medical imaging. To our best knowledge, the datasets that currently exist for aorta segmentation, usually only include the main part of the aorta (ascending aorta, aortic arch and part of the abdominal aorta), while other parts of the aorta and aortic branches are ignored. In addition, the training of deep learning models is a time-consuming process, which costs a lot of computing resources. Finally, Table 2 provides a compact overview of the reviewed papers according to which parts of the aortic vessel tree they segmented, and if and what kind of diseases, like calcification, aneurysm or dissection, was involved in these works. It also reveals that no work has targeted the intercostal arteries (label 8 in Figure 1) so far, which makes sense, because in most scans they are too small to be clearly defined, even manually, according to our medical partner. Nevertheless, we included them in our aortic vessel tree to be consistent with the original publication (Du et al. (2015)). In addition, future scanner generations may visualize them more reliably, and recent works already address this issue, for example, for intra-operative guidance during thoracic endovascular repair (Koutouzi et al. (2017)).

During our review, some issues emerged when comparing these aorta segmentation approaches from different studies. Although all studies introduced their validation datasets, most were based on private data from hospitals or medical institutes. No information is available about whether the different original images had similar qualities, and if their ground truth segmentation was based on similar standards, and what was the interoperator variability between ground truth annotators. This created difficulties in comparing the performance of their approaches. Additionally, as mentioned earlier,

their segmentation results were evaluated using various metrics, which are all statistical tools to measure the segmentation performance, but have different emphases and units. Therefore, it is impossible to objectively compare segmentation accuracy between studies that applied two different assessment metrics based only on published information.

In terms of methods, earlier research focused only on parts of the aortic vessel tree, and a certain degree of human interaction was necessary. Recently, more studies have segmented the aorta and its major branches, and also more studies have applied prior knowledge or deep learning algorithms to develop fully automated segmentation approaches.

Regarding the dataset, a variety of medical images have been collected for segmentation tasks in recent studies compared to previous ones. In addition, the amount of data collected for research, especially in deep learning studies, has also increased significantly.

Assessment methods have also changed. While it was initially difficult to compare segmentation approaches between different studies, in recent years, some major metrics (DSC, HD, MDE) have been widely applied. Researchers have consciously compared their methods with others, which accelerates the development of segmentation algorithms. Besides, some studies still have not mentioned their segmentation duration, which is actually an important factor considering the application of their segmentation methods.

Based on our review, currently the main challenges for aortic vessel tree segmentation are:

- Lack of common original datasets, which leads to difficulties in comparing the segmentation performance of different approaches;
- There is no gold standard for aorta segmentation tasks, which also causes difficulties when evaluating and comparing different segmentation approaches;
- Current annotation tools for medical images are not efficient enough to massively generate ground truth segmentation for training and evaluation;
- Medical images with high resolution showing the whole aorta cannot, in general, be directly inputted into neural networks. Solutions for this problem, like downsampling, usually reduce the accuracy of the segmentation results.

Finally, there is no common definition for a *stopping criteria*, especially for the branching vessels. This can differ between scans due to the scan quality, in-plane resolution, slice thickness, field of view (FOV), contrast agent (distribution), etc. For an quantitative evaluation, in particular for common segmentation metrics, however, a *stopping criteria* should be in a similar range for all scans to enable valid error calculating over the same length of each branching aortic artery.

## 6.2. Future Directions

Our study suggests that deep learning approaches have advantages in aorta segmentation tasks over traditional methods, especially considering automation and generalisation. The main limitation of these algorithms is the lack of datasets and corresponding ground truth annotations, which, when made public to the research community,



would also enable more groups to work on this problem and host public biomedical challenges, like the SegTHOR Challenge (Petitjean et al. (2019)), which included the main aorta in the thorax, but extended to the whole aortic vessel tree (including the abdominal aorta and the iliac arteries).

To the best of our knowledge, no approach has provided a concise and accurate solution for the segmentation of aortic vessel trees. Some future directions for these tasks could be:

- More datasets with well-annotated ground truths should be established and shared to help evaluate and compare different kinds of segmentation approaches;
- Classical approaches can be combined with deep learning algorithms to simplify the segmentation process and improve the automation;
- To avoid quality loss due to downsampling full body scans of the aorta to input them into neural networks, patch-based approaches should be investigated for the aorta;
- More public challenges, e.g. on Grand Challenge (<https://grand-challenge.org/>), that target aortic vessel tree segmentation tasks should be held to better compare and evaluate existing approaches.

### 6.3. *Final Remarks*

The aorta is the main artery of the human body, and its diseases pose a significant threat to human life. Computer-aided aorta segmentation is an important step in the detection and analysis of aortic diseases. We conducted a comprehensive introduction of existing aorta segmentation algorithms, as well as some vessel segmentation approaches. Furthermore, we identified the current challenges and future directions in this field. We believe our review provides a summarized reference for researchers who work or want to work in aorta-related medical imaging. In this regards, Table 2 provides a compact overview for researchers, which parts (but also diseases) of the aortic vessel tree have already been targeted by contributions, but also which have not yet been targeted by the research community. This enables researchers to quickly identify under-researched areas and applications within the aortic vessel tree.

The contribution of our review is threefold. We

- provided an overview of aortic diseases where aorta segmentation approaches can play a significant role;
- conducted a comprehensive introduction and comparison of existing aorta segmentation algorithms;
- provided directions for future work, including the development of segmentation technologies and the expansion of its application domain.

## Acknowledgments

This work received funding from the TU Graz Lead Project (Mechanics, Modeling and Simulation of Aortic Dissection), the Austrian Science Fund (FWF) KLI 678-B31: ‘enFaced: Virtual and Augmented Reality Training and Navigation Module for 3D-Printed Facial Defect Reconstructions’, and was supported by CAMEd (COMET K-Project 871132), which is funded by the Austrian Federal Ministry of Transport, Innovation and Technology (BMVIT), the Austrian Federal Ministry for Digital and Economic Affairs (BMDW) and the Styrian Business Promotion Agency (SFG). AFF was supported by the Royal Academy of Engineering (INSILEX CiET1819\19), and Engineering and Physical Sciences Research Council (TUSCA EP/V04799X/1). Further, we acknowledge CHB (Centre Henri Becquerel, 1 rue d’Amiens, 76038 Rouen, France). Finally, a collection of CTA scans including aortic vessel trees with corresponding segmentations (Radl et al. (2022a,b)), can be found and freely accessed on Figshare for research or informational purposes:  
Aortic Vessel Tree (AVT) CTA Datasets and Segmentations

## References

- Amorim, P., Moraes, T., Silva, J., Pedrini, H., 2015. Invesalius: An interactive rendering framework for health care support, in: International symposium on visual computing, Springer. pp. 45–54.
- Auer, M., Gasser, T.C., 2010. Reconstruction and finite element mesh generation of abdominal aortic aneurysms from computerized tomography angiography data with minimal user interactions. *IEEE Transactions on Medical Imaging* 29, 1022–1028. doi:10.1109/TMI.2009.2039579.
- Barrett, J.F., Keat, N., 2004. Artifacts in ct: recognition and avoidance. *Radiographics* 24, 1679–1691.
- Bauer, C., Pock, T., Sorantin, E., Bischof, H., Beichel, R., 2010. Segmentation of interwoven 3d tubular tree structures utilizing shape priors and graph cuts. *Medical image analysis* 14, 172–184.
- Berhane, H., Scott, M., Elbaz, M., Jarvis, K., McCarthy, P., Carr, J., Malaisrie, C., Avery, R., Barker, A.J., Robinson, J.D., Rigsby, C.K., Markl, M., 2020. Fully automated 3d aortic segmentation of 4d flow mri for hemodynamic analysis using deep learning. *Magn Reson Med*. doi:10.1002/mrm.28257.
- Bidhult, S., Hedström, E., Carlsson, M., Töger, J., Steding-Ehrenborg, K., Arheden, H., Aletras, A.H., Heiberg, E., 2019. A new vessel segmentation algorithm for robust blood flow quantification from two-dimensional phase-contrast magnetic resonance images. *Clinical Physiology and Functional Imaging* 39, 327–338. doi:10.1111/cpf.12582.
- Biesdorf, A., Worz, S., Tengg-Kobligh, H.V., Rohr, K., Schnorr, C., 2015. 3d segmentation of vessels by incremental implicit polynomial fitting and convex optimization, *IEEE Computer Society*. pp. 1540–1543. doi:10.1109/ISBI.2015.7164171.

- Biesdorf, A., Wörz, S., Müller, T., Weber, T.F., Heye, T., Hosch, W., Tengg-Kobligk, H.V., Rohr, K., 2011. Model-based segmentation and motion analysis of the thoracic aorta from 4d ecg-gated cta images, pp. 589–596. doi:10.1007/978-3-642-23623-5\_74.
- Bodur, O., Grady, L., Stillman, A., Setser, R., Funka-Lea, G., O'Donnell, T., 2007. Semi-automatic aortic aneurysm analysis, in: Manduca, A., Hu, X.P. (Eds.), *Medical Imaging 2007: Physiology, Function, and Structure from Medical Images*, International Society for Optics and Photonics. SPIE. pp. 454 – 463. URL: <https://doi.org/10.1117/12.710719>, doi:10.1117/12.710719.
- Bolger, A.F., 2008. Aortic intramural haematoma. *Heart* 94, 1670–1674. doi:10.1136/hrt.2007.132811.
- Boskamp, T., Rinck, D., Link, F., Kümmerlen, B., Stamm, G., Mildenerger, P., 2004. New vessel analysis tool for morphometric quantification and visualization of vessels in ct and mr imaging data sets. *Radiographics* 24, 287–297. doi:10.1148/rg.241035073.
- Boykov, Y., Veksler, O., Zabih, R., 2001. Fast approximate energy minimization via graph cuts. *IEEE Transactions on Pattern Analysis and Machine Intelligence* , 1222 – 1239doi:10.1109/34.969114.
- de Bruijne, M., Ginneken, B., Maintz, J., Niessen, W., Viergever, M., 2002. Active shape model based segmentation of abdominal aortic aneurysms in cta images. *Proceedings of SPIE - The International Society for Optical Engineering* 4684. doi:10.1117/12.467188.
- de Bruijne, M., Ginneken, B., Niessen, W., Loog, M., Viergever, M., 2003. Model-based segmentation of abdominal aortic aneurysms in cta images. *Proc SPIE* 5032. doi:10.1117/12.481367.
- Bruyninckx, P., Loeckx, D., Vandermeulen, D., Suetens, P., 2010. Segmentation of liver portal veins by global optimization, *SPIE*. p. 76241Z. doi:10.1117/12.843995.
- Bustamante, M., Petersson, S., Eriksson, J., Alehagen, U., Dyverfeldt, P., Carlhäll, C.J., Ebbens, T., 2015. Atlas-based analysis of 4d flow cmr: Automated vessel segmentation and flow quantification. *Journal of Cardiovascular Magnetic Resonance* 17. doi:10.1186/s12968-015-0190-5.
- Cao, L., Shi, R., Ge, Y., Xing, L., Zuo, P., Jia, Y., Liu, J., He, Y., Wang, X., Luan, S., Chai, X., Guo, W., 2019. Fully automatic segmentation of type b aortic dissection from cta images enabled by deep learning. *European Journal of Radiology* 121. doi:10.1016/j.ejrad.2019.108713.
- Chen, D., Mirebeau, J.M., Cohen, L.D., 2016. Vessel tree extraction using radius-lifted keypoints searching scheme and anisotropic fast marching method. *Journal of Algorithms and Computational Technology* 10, 224–234. doi:10.1177/1748301816656289.

- Chen, D., Zhang, X., Mei, Y., Liao, F., Xu, H., Li, Z., Xiao, Q., Guo, W., Zhang, H., Yan, T., Xiong, J., Ventikos, Y., 2021. Multi-stage learning for segmentation of aortic dissections using a prior aortic anatomy simplification. *Medical Image Analysis* 69. doi:10.1016/j.media.2020.101931.
- Cheung, W.K., Bell, R., Nair, A., Menezies, L., Patel, R., Wan, S., Chou, K., Chen, J., Torii, R., Davies, R.H., Moon, J.C., Alexander, D.C., Jacob, J., 2021. A computationally efficient approach to segmentation of the aorta and coronary arteries using deep learning. *medRxiv* doi:10.1101/2021.02.18.21252005.
- Çiçek, Ö., Abdulkadir, A., Lienkamp, S., Brox, T., Ronneberger, O., 2016. 3d u-net: Learning dense volumetric segmentation from sparse annotation. *International Conference on Medical Image Computing and Computer-Assisted Intervention* , 424–432.
- Codari, M., Pepe, A., Mistelbauer, G., Mastrodicasa, D., Walters, S., Willemink, M.J., Fleischmann, D., 2020. Deep reinforcement learning for localization of the aortic annulus in patients with aortic dissection, in: *International Workshop on Thoracic Image Analysis*, Springer. pp. 94–105.
- Das, B., Mallya, Y., Srikanth, S., Malladi, R., 2006. Aortic thrombus segmentation using narrow band active contour model, in: *International Conference of the IEEE Engineering in Medicine and Biology Society*. doi:10.1109/IEMBS.2006.4397423.
- Du, T., Hu, D., Cai, D., 2015. Outflow boundary conditions for blood flow in arterial trees. *PLoS ONE* 10. doi:10.1371/journal.pone.0128597.
- Duan, X., Shi, M., Wang, J., Zhao, H., Chen, D., 2016. Segmentation of the aortic dissection from CT images based on spatial continuity prior model, in: *2016 8th IEEE International Conference on Information Technology in Medicine and Education (ITME)*, pp. 275–280.
- Duquette, A.A., Jodoin, P.M., Bouchot, O., Lalande, A., 2012. 3d segmentation of abdominal aorta from ct-scan and mr images. *Computerized Medical Imaging and Graphics* 36, 294–303. doi:10.1016/j.compmedimag.2011.12.001.
- Egger, J., Freisleben, B., Setser, R., Renapuraar, R., Biermann, C., O'Donnell, T., 2009. Aorta segmentation for stent simulation. *MICCAI Workshop on Cardiovascular Interventional Imaging and Biophysical Modelling* .
- Egger, J., Grosskopf, S., Nimsky, C., Kapur, T., Freisleben, B., 2012. Modeling and visualization techniques for virtual stenting of aneurysms and stenoses. *Computerized Medical Imaging and Graphics* 36, 183–203.
- Egger, J., Mostarki, Z., Grobkopf, S., Freisleben, B., 2007. Preoperative measurement of aneurysms and stenosis and stentsimulation for endovascular treatment, in: *2007 4th IEEE International Symposium on Biomedical Imaging: From Nano to Macro*, pp. 392–395. doi:10.1109/ISBI.2007.356871.

- Egger, J., Mostarkic, Z., Grosskopf, S., Freisleben, B., 2007. A fast vessel centerline extraction algorithm for catheter simulation, in: Twentieth IEEE International Symposium on Computer-Based Medical Systems (CBMS'07), pp. 177–182. doi:10.1109/CBMS.2007.5.
- Erbel, R., Aboyans, V.e.a., 2014. 2014 esc guidelines on the diagnosis and treatment of aortic diseases. *European Heart Journal* 35, 2873–2926.
- Erhart, P., Hyhlik-Dürr, A., Geisbüsch, P., Kotelis, D., Müller-Eschner, M., Gasser, T., von Tengg-Kobligh, H., Böckler, D., 2015. Finite element analysis in asymptomatic, symptomatic, and ruptured abdominal aortic aneurysms: In search of new rupture risk predictors. *European Journal of Vascular and Endovascular Surgery* 49, 239–245. URL: <https://www.sciencedirect.com/science/article/pii/S1078588414006376>, doi:<https://doi.org/10.1016/j.ejvs.2014.11.010>.
- Fantazzini, A., Esposito, M., Finotello, A., Auricchio, F., Pane, B., Basso, C., Spinella, G., Conti, M., 2020. 3d automatic segmentation of aortic computed tomography angiography combining multi-view 2d convolutional neural networks. *Cardiovascular Engineering and Technology* 11, 576–586. doi:10.1007/s13239-020-00481-z.
- Frangi, A.F., Niessen, W.J., Vincken, K.L., Viergever, M.A., 1998. Multiscale vessel enhancement filtering, in: Wells, W.M., Colchester, A., Delp, S. (Eds.), *Medical Image Computing and Computer-Assisted Intervention — MICCAI'98*, Springer Berlin Heidelberg, Berlin, Heidelberg. pp. 130–137.
- Freiman, M., Joskowicz, L., Broide, N., Natanzon, M., Nammer, E., Shilon, O., Weizman, L., Sosna, J., 2012. Carotid vasculature modeling from patient ct angiography studies for interventional procedures simulation. *International Journal of Computer Assisted Radiology and Surgery* 7, 799–812. doi:10.1007/s11548-012-0673-x.
- Gallagher, M.J., Raff, G.L., 2008. Use of multislice ct for the evaluation of emergency room patients with chest pain: the so-called “triple rule-out”. *Catheterization and cardiovascular interventions* 71, 92–99.
- Gamechi, Z.S., Bons, L.R., Giordano, M., Bos, D., Budde, R.P., Kofoed, K.F., Pedersen, J.H., Roos-Hesselink, J.W., de Bruijne, M., 2019. Automated 3d segmentation and diameter measurement of the thoracic aorta on non-contrast enhanced ct. *European Radiology* 29, 4613–4623. doi:10.1007/s00330-018-5931-z.
- Gao, X., Kitslaar, P.H., Budde, R.P., Tu, S., de Graaf, M.A., Xu, L., Xu, B., Scholte, A.J., Dijkstra, J., Reiber, J.H., 2016. Automatic detection of aorto-femoral vessel trajectory from whole-body computed tomography angiography data sets. *International Journal of Cardiovascular Imaging* 32, 1311–1322. doi:10.1007/s10554-016-0901-5.
- Hager, A., Kanz, S., Kaemmerer, H., Schreiber, C., Hess, J., 2007. Coarctation long-term assessment (coala): Significance of arterial hypertension in a cohort of 404 patients up to 27 years after surgical repair of isolated coarctation of the aorta, even in the absence of restenosis and prosthetic material. *Journal of Thoracic and Cardiovascular Surgery* 134. doi:10.1016/j.jtcvs.2007.04.027.

- Hahn, L., Mistelbauer, G., Higashigaito, K., Koci, M., Willemink, M., Sailer, A., Fischbein, M., Fleischmann, D., 2020. Ct-based true- and false-lumen segmentation in type b aortic dissection using machine learning. *Radiology: Cardiothoracic Imaging* 2, e190179. doi:10.1148/ryct.2020190179.
- Harris, K.M., Braverman, A.C., Eagle, K.A., Woznicki, E.M., Pyeritz, R.E., Myrmel, T., Peterson, M.D., Voehringer, M., Fattori, R., Januzzi, J.L., Gilon, D., Montgomery, D.G., Nienaber, C.A., Trimarchi, S., Isselbacher, E.M., Evangelista, A., 2012. Acute aortic intramural hematoma: An analysis from the international registry of acute aortic dissection. *Circulation* 126. doi:10.1161/CIRCULATIONAHA.111.084541.
- Heimann, T., van Ginneken, B., Styner, M.A., Arzhaeva, Y., Aurich, V., Bauer, C., Beck, A., Becker, C., Beichel, R., Bekes, G., Bello, F., Binnig, G., Bischof, H., Bornik, A., Cashman, P.M.M., Chi, Y., Cordova, A., Dawant, B.M., Fidrich, M., Furst, J.D., Furukawa, D., Grenacher, L., Horneegger, J., Kainmueller, D., Kitney, R.I., Kobatake, H., Lamecker, H., Lange, T., Lee, J., Lennon, B., Li, R., Li, S., Meinzer, H., Nemeth, G., Raicu, D.S., Rau, A., van Rikxoort, E.M., Rousson, M., Rusko, L., Saddi, K.A., Schmidt, G., Seghers, D., Shimizu, A., Slagmolen, P., Sorantin, E., Soza, G., Susomboon, R., Waite, J.M., Wimmer, A., Wolf, I., 2009. Comparison and evaluation of methods for liver segmentation from ct datasets. *IEEE Transactions on Medical Imaging* 28, 1251–1265. doi:10.1109/TMI.2009.2013851.
- Hepp, T., Fischer, M., Winkelmann, M.T., Baldenhofer, S., Kuestner, T., Nikolaou, K., Yang, B., Gatidis, S., 2020. Fully automated segmentation and shape analysis of the thoracic aorta in non-contrast-enhanced magnetic resonance images of the german national cohort study. *J Thorac Imaging* doi:10.1097/RTI.0000000000000522.
- Herment, A., Kachenoura, N., Lefort, M., Bensalah, M., Dogui, A., Frouin, F., Mousseaux, E., Cesare, A.D., 2010. Automated segmentation of the aorta from phase contrast mr images: Validation against expert tracing in healthy volunteers and in patients with a dilated aorta. *Journal of Magnetic Resonance Imaging* 31, 881–888. doi:10.1002/jmri.22124.
- Hesamian, M., Jia, W., He, X., Kennedy, P., 2019. Deep learning techniques for medical image segmentation: Achievements and challenges. *Journal of Digital Imaging* , 582–596.
- Howard, J.P., Zaman, S., Ragavan, A., Hall, K., Leonard, G., Sutanto, S., Ramadoss, V., Razvi, Y., Linton, N.F., Bharath, A., Shun-Shin, M., Rueckert, D., Francis, D., Cole, G., 2020. Automated analysis and detection of abnormalities in transaxial anatomical cardiovascular magnetic resonance images: a proof of concept study with potential to optimize image acquisition. *The International Journal of Cardiovascular Imaging* URL: <http://link.springer.com/10.1007/s10554-020-02050-w>, doi:10.1007/s10554-020-02050-w.
- Jin, Y., Pepe, A., Li, J., Gsaxner, C., Egger, J., 2021. Deep learning and particle filter-based aortic dissection vessel tree segmentation, in: *Medical Imaging 2021*:

- Biomedical Applications in Molecular, Structural, and Functional Imaging, International Society for Optics and Photonics. p. 6.
- Kass, M., Witkin, A., Terzopoulos, D., 1988. Snakes: Active contour models. *International journal of computer vision* 1, 321–331.
- Khan, I.A., Nair, C.K., 2002. Clinical, diagnostic, and management perspectives of aortic dissection. *Chest* 122 (1), 311–328.
- Kim, H.C., Seol, Y., Choi, S., Oh, J., Kim, M., Sun, K., 2007. A study of aaa image segmentation technique using geometric active contour model with morphological gradient edge function. *Conference proceedings : ... Annual International Conference of the IEEE Engineering in Medicine and Biology Society. IEEE Engineering in Medicine and Biology Society. Conference 2007*, 4437–40. doi:10.1109/IEMBS.2007.4353323.
- Kirişli, H.e.a., 2010. Evaluation of a multi-atlas based method for segmentation of cardiac cta data: a large-scale, multicenter, and multivendor study. *Medical Physics* doi:10.1118/1.3512795.
- Kosasih, R., 2020. Automatic segmentation of abdominal aortic aneurism (aaa) by using active contour models. *Scientific Journal of Informatics* 7, 2407–7658. URL: <http://journal.unnes.ac.id/nju/index.php/sji>.
- Koutouzi, G., Sandström, C., Skoog, P., Roos, H., Falkenberg, M., 2017. 3d image fusion to localise intercostal arteries during tevar. *EJVES short reports* 35, 7–10.
- Krissian, K., Carreira, J.M., Esclarin, J., Maynar, M., 2014. Semi-automatic segmentation and detection of aorta dissection wall in MDCT angiography. *Medical Image Analysis* 18 (1), 83–102.
- Krissian, K., Malandain, G., Ayache, N., Vaillant, R., Troussset, Y., 2000. Model-based detection of tubular structures in 3d images. *Computer vision and image understanding* 80, 130–171.
- Kurugol, S., Come, C.E., Diaz, A.A., Ross, J.C., Kinney, G.L., Black-Shinn, J.L., Hokanson, J.E., Budoff, M.J., Washko, G.R., Estepar, R.S.J., 2015. Automated quantitative 3d analysis of aorta size, morphology, and mural calcification distributions. *Medical Physics* 42, 5467–5478. doi:10.1118/1.4924500.
- Lambert, Z., Petitjean, C., Dubray, B., Kuan, S., 2020. Segthor: Segmentation of thoracic organs at risk in ct images, in: *2020 Tenth International Conference on Image Processing Theory, Tools and Applications (IPTA), IEEE*. pp. 1–6.
- Lareyre, F., Adam, C., Carrier, M., Dommerc, C., Mialhe, C., Raffort, J., 2019. A fully automated pipeline for mining abdominal aortic aneurysm using image segmentation. *Scientific Reports* 9. doi:10.1038/s41598-019-50251-8.
- Lawonn, K., Smit, N.N., Bühler, K., Preim, B., 2018. A survey on multimodal medical data visualization, in: *Computer Graphics Forum, Wiley Online Library*. pp. 413–438.

- Lee, S.H., Kang, J., Lee, S., 2017. Enhanced particle-filtering framework for vessel segmentation and tracking. *Computer Methods and Programs in Biomedicine* 148, 99–112. doi:10.1016/j.cmpb.2017.06.017.
- LeMaire, S.A., Russel, L., 2011. Epidemiology of thoracic aortic dissection. *Nature Reviews Cardiology* 8, 103–113.
- Levy, D., Goyal, A., Grigorova, Y., Farci, F., Le, J.K., 2022. Aortic dissection, in: StatPearls [Internet]. StatPearls publishing.
- Li, J., Cao, L., Cheng, W., Bowen, M., Guo, W., 2018. Towards automatic measurement of type B aortic dissection parameters: Methods, applications and perspective, in: *Intravascular Imaging and Computer Assisted Stenting and Large-Scale Annotation of Biomedical Data and Expert Label Synthesis*, Springer International Publishing, Cham. pp. 64–72.
- Li, K., Wu, X., Chen, D.Z., Sonka, M., 2006. Optimal surface segmentation in volumetric images-a graph-theoretic approach. *IEEE Transactions on Pattern Analysis and Machine Intelligence* 28, 119–134. doi:10.1109/TPAMI.2006.19.
- Li, Z., Feng, J., Feng, Z., An, Y., Gao, Y., Lu, B., Zhou, J., 2019. Lumen segmentation of aortic dissection with cascaded convolutional network, Springer Verlag. pp. 122–130. doi:10.1007/978-3-030-12029-0\_14.
- Litjens, G., Kooi, T., Bejnordi, B.E., Setio, A.A.A., Ciompi, F., Ghafoorian, M., van der Laak, J.A.W.M., van Ginneken, B., Sánchez, C.I., 2017. A survey on deep learning in medical image analysis URL: <http://arxiv.org/abs/1702.05747><http://dx.doi.org/10.1016/j.media.2017.07.005>, doi:10.1016/j.media.2017.07.005.
- Loncaric, S., Subasic, M., Sorantin, E., 2000. 3-d deformable model for abdominal aortic aneurysm segmentation from ct images, pp. 139 – 144. doi:10.1109/ISPA.2000.914904.
- Long, J., Shelhamer, E., Darrell, T., 2014. Fully convolutional networks for semantic segmentation. CoRR abs/1411.4038. URL: <http://arxiv.org/abs/1411.4038>.
- López-Linares, K., Aranjuelo, N., Kabongo, L., Maclair, G., Lete, N., Ceresa, M., García-Familiar, A., Macía, I., Ballester, M.A.G., 2018. Fully automatic detection and segmentation of abdominal aortic thrombus in post-operative cta images using deep convolutional neural networks. *Medical Image Analysis* 46, 202–214. doi:10.1016/j.media.2018.03.010.
- Martínez-Mera, J.A., Tahoces, P.G., Carreira, J.M., 2013. A hybrid method based on level set and 3D region growing for segmentation of the thoracic aorta. *Computer Aided Surgery* 18(5-6), 109–117.
- Maton, A., Hopkins, J., McLaughlin, C.W., Johnson, S., Warner, M.Q., LaHart, D., Wright, J.D., 1995. *Human Biology Health*. Englewood Cliffs, New Jersey: Prentice Hall.



- Mistelbauer, G., Schmidt, J., Sailer, A., Bäumler, K., Walters, S., Fleischmann, D., 2016. Aortic dissection maps: comprehensive visualization of aortic dissections for risk assessment, in: VCBM '16: Proceedings of the Eurographics Workshop on Visual Computing for Biology and Medicine, p. 143–152.
- Moccia, S., di Milano, E.D.M.P., Mattos, L.S., Momi, E.D., Hadji, S.E., 2018. Blood vessel segmentation algorithms-review of methods, datasets and evaluation metrics. URL: <https://www.researchgate.net/publication/331299499>.
- Morais, P., Vilaça, J.L., Queirós, S., Bourier, F., Deisenhofer, I., Tavares, J.M.R., D'hooge, J., 2017. A competitive strategy for atrial and aortic tract segmentation based on deformable models. *Medical Image Analysis* 42, 102–116. doi:10.1016/j.media.2017.07.007.
- Morris, E.D., Ghanem, A.I., Pantelic, M.V., Walker, E.M., Han, X., Glide-Hurst, C.K., 2019. Cardiac substructure segmentation and dosimetry using a novel hybrid magnetic resonance and computed tomography cardiac atlas. *International Journal of Radiation Oncology Biology Physics* 103, 985–993. doi:10.1016/j.ijrobp.2018.11.025.
- Nienaber, C.A., 2013. The role of imaging in acute aortic syndromes. *European Heart Journal Cardiovascular Imaging* 14, 15–23. doi:10.1093/ehjci/jes215.
- Nienaber, C.A., Clough, R.E., Sakalihasan, N., Suzuki, T., Gibbs, R., Mussa, F., Jenkins, M.P., Thompson, M.M., Evangelista, A., Yeh, J.S., Cheshire, N., Rosendahl, U., Pepper, J., 2016. Aortic dissection. *Nature Reviews Disease Primers* 21, 16053.
- Olabarriaga, S., Rouet, j.m., Fradkin, M., Breeuwer, M., Niessen, W., 2005. Segmentation of thrombus in abdominal aortic aneurysms from cta with non-parametric statistical grey level appearance modelling. *IEEE transactions on medical imaging* 24, 477–85. doi:10.1109/TMI.2004.843260.
- Osada, H., Kyogoku, M., Matsuo, T., Kanemitsu, N., 2018. Histopathological evaluation of aortic dissection: a comparison of congenital versus acquired aortic wall weakness. *Interactive CardioVascular and Thoracic Surgery* 27, 277–283.
- Pepe, A., Li, J., Rolf-Pissarczyk, M., Gsaxner, C., Chen, X., Holzapfel, G.A., Egger, J., 2020. Detection, segmentation, simulation and visualization of aortic dissections: A review. *Medical Image Analysis* 65. doi:10.1016/j.media.2020.101773.
- Petitjean, C., Ruan, S., Lambert, Z., Dubray, B. (Eds.), 2019. Proceedings of the 2019 Challenge on Segmentation of THoracic Organs at Risk in CT Images, SegTHOR@ISBI 2019, April 8, 2019. volume 2349 of *CEUR Workshop Proceedings*, CEUR-WS.org. URL: <http://ceur-ws.org/Vol-2349>.
- Pinheiro, P.O., Lin, T.Y., Collobert, R., Dollár, P., 2016. Learning to refine object segments, in: Leibe, B., Matas, J., Sebe, N., Welling, M. (Eds.), *Computer Vision – ECCV 2016*, Springer International Publishing, Cham. pp. 75–91.

- Pock, T., Beichel, R., Bischof, H., 2005. A novel robust tube detection filter for 3d centerline extraction, in: *Scandinavian Conference on Image Analysis*, Springer. pp. 481–490.
- Radl, L., Jin, Y., Pepe, A., Li, J., Gsaxner, C., hua Zhao, F., Egger, J., 2022a. Aortic Vessel Tree (AVT) CTA Datasets and Segmentations URL: [https://figshare.com/articles/dataset/Aortic\\_Vessel\\_Tree\\_AVT\\_CTA\\_Datasets\\_and\\_Segmentations/14806362](https://figshare.com/articles/dataset/Aortic_Vessel_Tree_AVT_CTA_Datasets_and_Segmentations/14806362), doi:10.6084/m9.figshare.14806362.v1.
- Radl, L., Jin, Y., Pepe, A., Li, J., Gsaxner, C., Zhao, F.h., Egger, J., 2022b. Avt: Multicenter aortic vessel tree cta dataset collection with ground truth segmentation masks. *Data in Brief*, 107801.
- Ritter, F., Hansen, C., Dicken, V., Konrad, O., Preim, B., Peitgen, H.O., 2006. Real-time illustration of vascular structures. *IEEE Transactions on Visualization and Computer Graphics* 12, 877–884.
- Robben, D., Türetken, E., Sunaert, S., Thijs, V., Wilms, G., Fua, P., Maes, F., Suetens, P., 2014. Lncs 8673 - simultaneous segmentation and anatomical labeling of the cerebral vasculature.
- Rogers, A.M., Hermann, L.K., Booher, A.M., Nienaber, C.A., Williams, D.M., Kazerouni, E.A., Froehlich, J.B., O’Gara, P.T., Montgomery, D.G., Cooper, J.V., Harris, K.M., Hutchison, S., Evangelista, A., Isselbacher, E.M., Eagle, K.A., 2011. Sensitivity of the aortic dissection detection risk score, a novel guideline-based tool for identification of acute aortic dissection at initial presentation: Results from the international registry of acute aortic dissection. *Circulation* 123, 2213–2218. doi:10.1161/CIRCULATIONAHA.110.988568.
- Ronneberger, O., Fischer, P., Brox, T., 2015. U-net: Convolutional networks for biomedical image segmentation. *CoRR abs/1505.04597*. URL: <http://arxiv.org/abs/1505.04597>.
- Rueckert, D., Burger, P., Forbat, S.M., Mohiaddin, R.D., Yang, G.Z., 1997. Automatic tracking of the aorta in cardiovascular mr images using deformable models. *IEEE Transactions on Medical Imaging* 16, 581–590. doi:10.1109/42.640747.
- Schmied, M., Pepe, A., Egger, J., 2021. A patch-based-approach for aortic landmarking, in: *Medical Imaging 2021: Biomedical Applications in Molecular, Structural, and Functional Imaging*, International Society for Optics and Photonics. p. 1160010.
- Selver, M.A., Kavur, A.E., 2016. Implementation and use of 3d pairwise geodesic distance fields for seeding abdominal aortic vessels. *International Journal of Computer Assisted Radiology and Surgery* 11, 803–816. doi:10.1007/s11548-015-1321-z.
- Sethian, J.A., Vladimirsky, A., 2000. Fast methods for the eikonal and related hamilton– jacobi equations on unstructured meshes. *Proceedings of the National Academy of Sciences* 97, 5699–5703. URL: <https://>

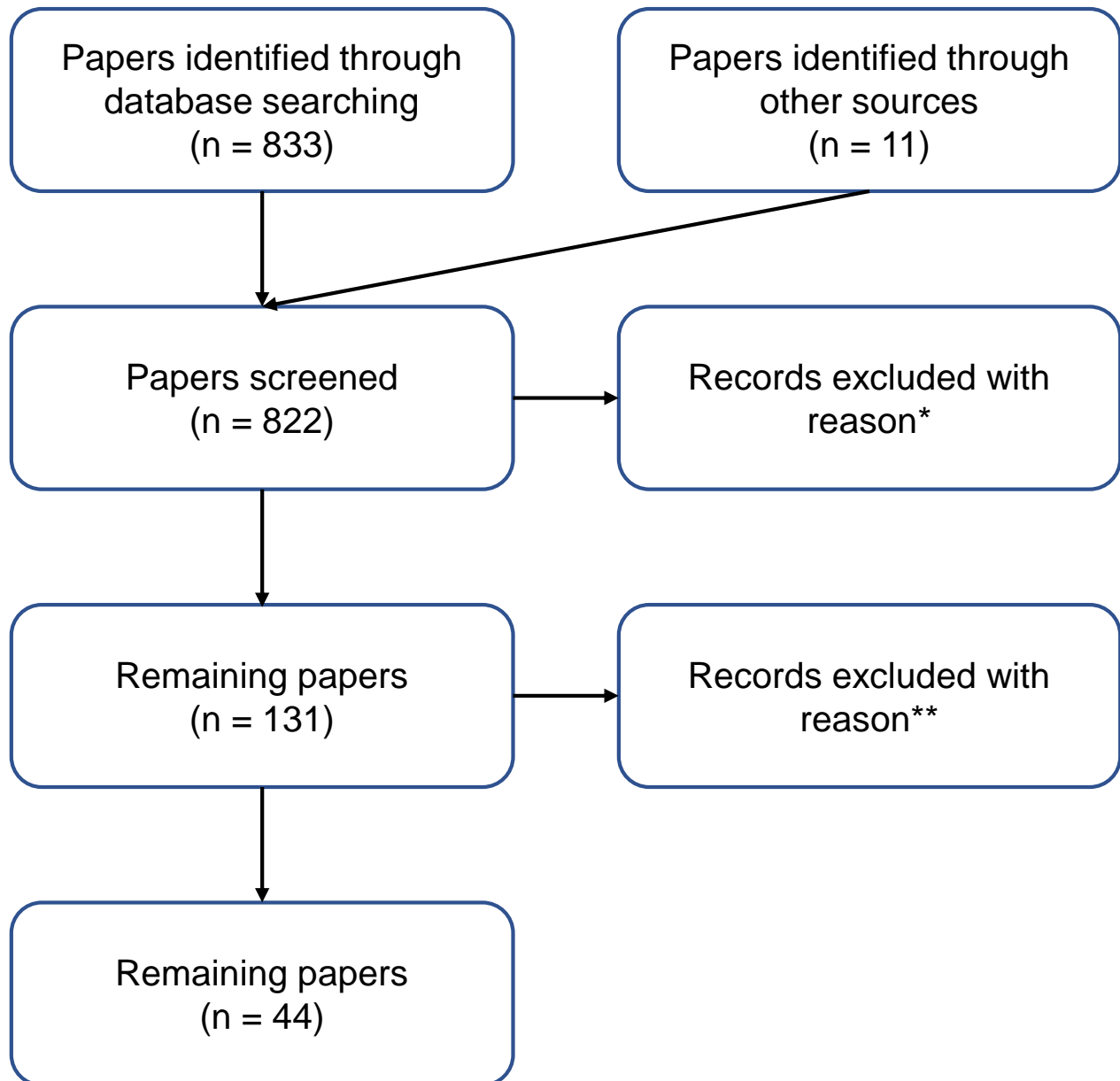
- [//www.pnas.org/content/97/11/5699](https://www.pnas.org/content/97/11/5699), doi:10.1073/pnas.090060097, arXiv:<https://www.pnas.org/content/97/11/5699.full.pdf>.
- Shahzad, R., Dzyubachyk, O., Staring, M., Kullberg, J., Johansson, L., Ahlström, H., Lelieveldt, B.P., van der Geest, R.J., 2015. Automated extraction and labelling of the arterial tree from whole-body mra data. *Medical Image Analysis* 24, 28–40. URL: <https://www.sciencedirect.com/science/article/pii/S1361841515000754>, doi:<https://doi.org/10.1016/j.media.2015.05.008>.
- Shamseer, L., Moher, D., Clarke, M., Ghersi, D., Liberati, A., Petticrew, M., Shekelle, P., Stewart, L.A., 2015. Preferred reporting items for systematic review and meta-analysis protocols (prisma-p) 2015: elaboration and explanation. *BMJ* 349. URL: <https://www.bmj.com/content/349/bmj.g7647>, doi:10.1136/bmj.g7647, arXiv:<https://www.bmj.com/content/349/bmj.g7647.full.pdf>.
- Shen, D., Wu, G., Suk, H.I., 2017. Deep learning in medical image analysis. *Annual review of biomedical engineering* 19, 221–248.
- Sieren, M.M., Widmann, C., Weiss, N., Moltz, J.H., Link, F., Wegner, F., Stahlberg, E., Horn, M., Oecherting, T.H., Goltz, J.P., Barkhausen, J., Frydrychowicz, A., 2022. Automated segmentation and quantification of the healthy and diseased aorta in ct angiographies using a dedicated deep learning approach. *Eur Radiol* 32, 690–701. doi:10.1007/s00330-021-08130-2.
- Simpson, A.L., Antonelli, M., Bakas, S., Bilello, M., Farahani, K., van Ginneken, B., Kopp-Schneider, A., Landman, B.A., Litjens, G., Menze, B., Ronneberger, O., Summers, R.M., Bilic, P., Christ, P.F., Do, R.K.G., Gollub, M., Golia-Pernicka, J., Heckers, S.H., Jarnagin, W.R., McHugo, M.K., Napel, S., Vorontsov, E., Maier-Hein, L., Cardoso, M.J., 2019. A large annotated medical image dataset for the development and evaluation of segmentation algorithms. arXiv:1902.09063.
- Sreejini, K.S., Govindan, V.K., 2015. Improved multiscale matched filter for retina vessel segmentation using pso algorithm. *Egyptian Informatics Journal* 16, 253–260. doi:10.1016/j.eij.2015.06.004.
- Subasic, M., Loncaric, S., Sorantin, E., 2000. 3-d image analysis of abdominal aortic aneurysm, in: *Medical Infobahn for Europe*. IOS Press, pp. 1195–1200.
- Subramanian, K., Steinmiller, M., Sifri, D., Boll, D., 2003. Automatic aortic vessel tree extraction and thrombus detection in multislice CT, in: Sonka, M., Fitzpatrick, J.M. (Eds.), *Medical Imaging 2003: Image Processing*, International Society for Optics and Photonics. SPIE. pp. 1629 – 1638. URL: <https://doi.org/10.1117/12.483542>.
- Taha, A.A., Hanbury, A., 2015. Metrics for evaluating 3d medical image segmentation: analysis, selection, and tool. *BMC medical imaging* 15, 1–28.

- Tahoces, P.G., Alvarez, L., González, E., Cuenca, C., Trujillo, A., Santana-Cedrés, D., Esclarín, J., Gomez, L., Mazorra, L., Alemán-Flores, M., Carreira, J.M., 2019. Automatic estimation of the aortic lumen geometry by ellipse tracking. *International Journal of Computer Assisted Radiology and Surgery* 14, 345–355. doi:10.1007/s11548-018-1861-0.
- Tang, H., van Walsum, T., van Onkelen, R.S., Hameeteman, R., Klein, S., Schaap, M., Tori, F.L., van den Bouwhuijsen, Q.J., Witteman, J.C., van der Lugt, A., van Vliet, L.J., Niessen, W.J., 2012. Semiautomatic carotid lumen segmentation for quantification of lumen geometry in multispectral mri. *Medical Image Analysis* 16, 1202–1215. doi:10.1016/j.media.2012.05.014.
- Terzopoulos, D., Metaxas, D., 1991. Dynamic 3d models with local and global deformations: deformable superquadrics. *IEEE Transactions on Pattern Analysis and Machine Intelligence* 13, 703–714. doi:10.1109/34.85659.
- Tortora, G.J., Nielsen, M.T., 2016. *Principles of Human Anatomy*, 14th Edition. WILEY.
- Trullo, R., Petitjean, C., Ruan, S., Dubray, B., Nie, D., Shen, D., 2017. Segmentation of organs at risk in thoracic ct images using a sharpmask architecture and conditional random fields, *IEEE Computer Society*. pp. 1003–1006. doi:10.1109/ISBI.2017.7950685.
- Tsai, T.T., Nienaber, C.A., Eagle, K.A., 2005. Acute aortic syndromes. *Circulation* 112, 3802–3813.
- Volonghi, P., Tresoldi, D., Cadioli, M., Uselli, A.M., Ponzini, R., Morbiducci, U., Esposito, A., Rizzo, G., 2016. Automatic extraction of three-dimensional thoracic aorta geometric model from phase contrast mri for morphometric and hemodynamic characterization. *Magnetic Resonance in Medicine* 75, 873–882. doi:10.1002/mrm.25630.
- Wang, X., Heimann, T., Lo, P., Sumkauskaitė, M., Puderbach, M., de Bruijne, M., Meinzer, H.P., Wegner, I., 2012. Statistical tracking of tree-like tubular structures with efficient branching detection in 3d medical image data. *Physics in medicine and biology* 57, 5325–5342. doi:10.1088/0031-9155/57/16/5325.
- Wang, Y., Seguro, F., Kao, E., Zhang, Y., Faraji, F., Zhu, C., Haraldsson, H., Hope, M., Saloner, D., Liu, J., 2017. Segmentation of lumen and outer wall of abdominal aortic aneurysms from 3d black-blood mri with a registration based geodesic active contour model. *Medical Image Analysis* 40, 1–10. doi:10.1016/j.media.2017.05.005.
- Wu, D., Shen, Y.H., Russell, L., Coselli, J.S., LeMaire, S.A., 2013. Molecular mechanisms of thoracic aortic dissection. *Journal of Surgical Research* 184, 907–924.
- Xie, Y., Padgett, J., Biancardi, A.M., Reeves, A.P., 2014. Automated aorta segmentation in low-dose chest ct images. *International Journal of Computer Assisted Radiology and Surgery* 9, 211–219. doi:10.1007/s11548-013-0924-5.

- Yu, Y., Gao, Y., Wei, J., Liao, F., Xiao, Q., Zhang, J., Yin, W., Lu, B., 2021. A three-dimensional deep convolutional neural network for automatic segmentation and diameter measurement of type b aortic dissection. *Korean journal of radiology* 22, 168–178. doi:10.3348/kjr.2020.0313.
- Zhao, J., Zhao, J., Pang, S., Feng, Q., 2022. Segmentation of the true lumen of aorta dissection via morphology-constrained stepwise deep mesh regression. *IEEE Transactions on Medical Imaging* 41, 1826–1836. doi:10.1109/TMI.2022.3150005.
- Zheng, Y., John, M., Liao, R., Boese, J., Kirschstein, U., Georgescu, B., Zhou, S.K., Kempfert, J., Walther, T., Brockmann, G., Comaniciu, D., 2010. Automatic aorta segmentation and valve landmark detection in c-arm ct: Application to aortic valve implantation, pp. 476–483. doi:10.1007/978-3-642-15705-9\_58.
- Zhong, J., Bian, Z., Hatt, C.R., Burris, N.S., 2021. Segmentation of the thoracic aorta using an attention-gated u-net, in: Mazurowski, M.A., Drukker, K. (Eds.), *Medical Imaging 2021: Computer-Aided Diagnosis*, International Society for Optics and Photonics. SPIE. pp. 147 – 153. URL: <https://doi.org/10.1117/12.2581947>, doi:10.1117/12.2581947.
- Zhuge, F., Rubin, G., Sun, S., Napel, S., 2006. An abdominal aortic aneurysm segmentation method: Level set with region and statistical information. *Medical physics* 33, 1440–53. doi:10.1118/1.2193247.

# **SUPPLEMENTARY MATERIAL**

## Flow Diagram



\*The reason for exclusion was for example a pure clinical contribution of the article, such as aorta measurements and medical findings.

\*\* The reason for exclusion was the overlap of contents with other papers or the lack of quantitative segmentation results.

**SEARCH ENGINES:**

IEEE Xplore, PubMed, Google Scholar and ScienceDirect

Keywords:

'aorta' AND 'segmentation' [Title/Abstract]

Date of search: January 2023

**IEEE Xplore: 110**

**PubMed: 450**

**Google Scholar\*: 142**

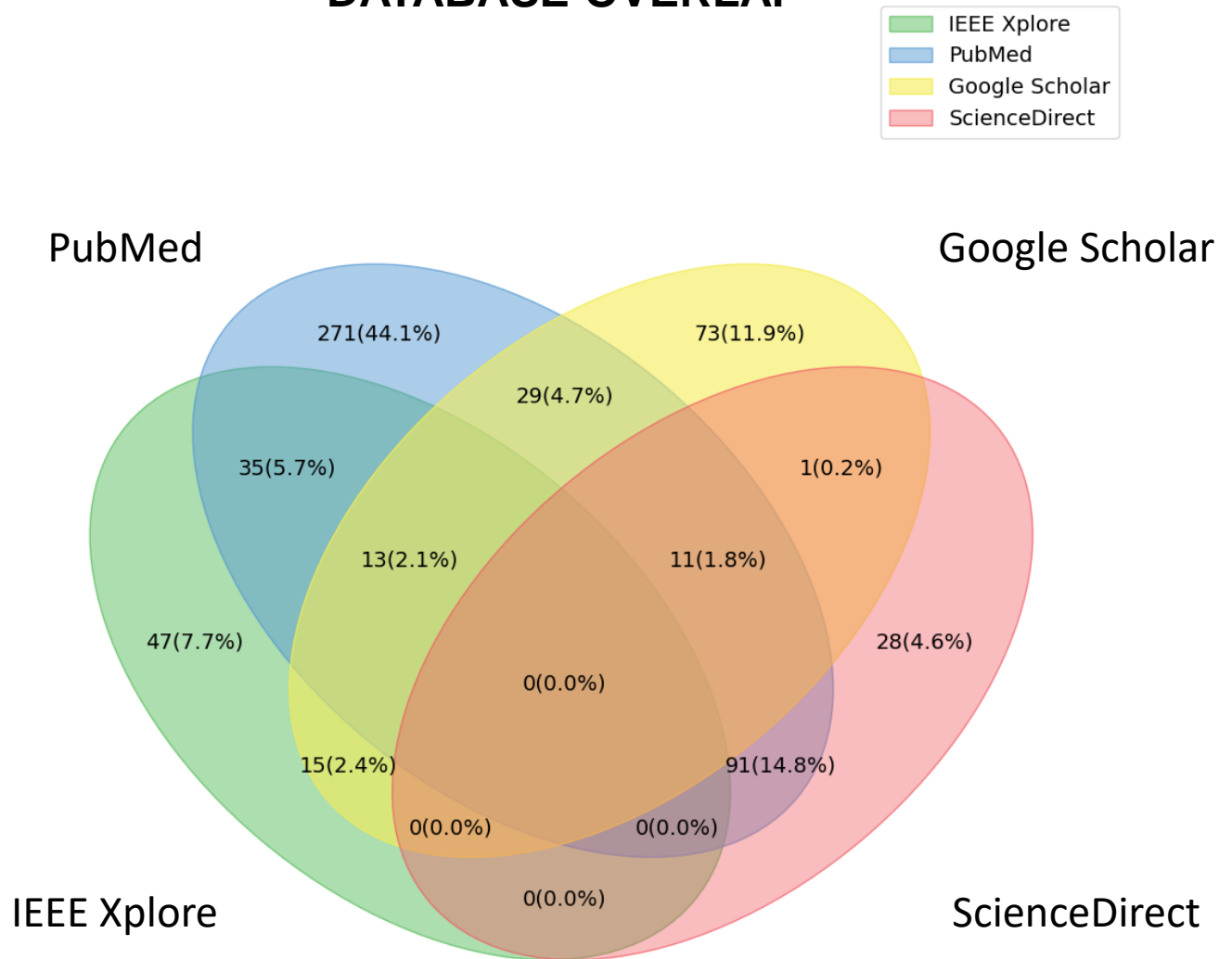
**ScienceDirect: 131**

**TOTAL: 833**

\*Differently than other engines, Google Scholar also searches in text and references. Therefore, only in this specific case, each search was filtered with the operator 'allintitle', e.g., allintitle: aorta segmentation.



# DATABASE OVERLAP



**Overall distribution after screening of the articles retrieved from the four databases and relative overlapping.**